AFD Thermosensory Neurons Mediate Tactile-Dependent Locomotion Modulation in *C. elegans*

Manuel Rosero[1,2] and Jihong Bai[1,2,#]

[1] Basic Sciences Division, Fred Hutchinson Cancer Center, Seattle, WA 98109

[2] Molecular and Cellular Biology Graduate Program, University of Washington, Seattle, WA 98109

[#] Jihong Bai, Ph.D. (Corresponding author)
Basic Sciences Division
Fred Hutchinson Cancer Center
1100 Fairview Ave N.
Seattle, WA 98109, USA
Email: jbai@fredhutch.org

ABSTRACT

Sensory neurons drive animal behaviors by detecting environmental stimuli and relaying information to downstream circuits. Beyond their primary roles in sensing, these neurons often form additional synaptic connections outside their main sensory modality, suggesting broader contributions to behavior modulation. Here, we uncover an unexpected role for the thermosensory neuron AFD in coupling tactile experience to locomotion modulation in *Caenorhabditis elegans*. We show that while AFD employs cGMP signaling for both thermotaxis and tactile-dependent modulation, the specific molecular components of the cGMP pathway differ between these two processes. Interestingly, disrupting the dendritic sensory apparatus of AFD, which is essential for thermotaxis, does not impair tactile-based locomotion modulation, indicating that AFD can mediate tactile-dependent behavior independently of its thermosensory apparatus. In contrast, ablating the AFD neuron eliminates tactile-dependent modulation, pointing to an essential role for AFD itself, rather than its sensory dendritic endings. Further, we find tactile-dependent modulation requires the AIB interneuron, which connects AFD to touch circuits via electrical synapses. Removing innexins expressed in AFD and AIB abolishes this modulation, while re-establishing AFD-AIB connections with engineered electrical synapses restores it. Collectively, these findings uncover a previously unrecognized function of AFD beyond thermosensation, highlighting its influence on context-dependent neuroplasticity and behavioral modulation through broader circuit connectivity.

INTRODUCTION

Adaptive behavioral responses require animals to interpret sensory signals in the context of prior experiences, enabling effective responses to changing environmental conditions. For example, rodents associate contextual cues, such as odors and colors, with rewards or punishments, leading to context-dependent adjustments in approach or avoidance behaviors [1,2]. Disruptions in the biological processes underlying this plasticity, as seen in neurological and psychiatric disorders, often result in impaired behavior modulation based on prior sensory experiences [3–7]. Recognizing the critical role of context-dependent behavioral modulation for survival and well-being, ongoing research focuses on uncovering the neuroplastic mechanisms responsible for these adaptive processes.

Studies across diverse organisms reveal that animals, regardless of nervous system complexity, integrate prior sensory experiences to shape behavior [8–15]. In the nematode *C. elegans*, which has only 302 neurons, locomotion strategies are modified by prior exposure to stimuli such as odors, touch, light, and starvation, demonstrating robust adaptive behaviors [16–23]. The wide range of adaptive behaviors, combined with the well-mapped *C. elegans* nervous system and abundant genetic tools, have empowered the discovery of fundamental circuit mechanisms and molecular pathways underlying context-dependent behavioral modulation [24–28].

The *C. elegans* sensory system comprises 60 ciliated sensory neurons specialized in detecting chemical, thermal, mechanical, and olfactory stimuli [29,30]. Each sensory neuron has a dendritic apparatus that converts specific environmental signals into neuronal activity, which drives signal flow through downstream networks of interneurons and motor neurons, ultimately shaping behavior [31–33]. Among these, AFD, a pair of bilaterally symmetric left-right neurons, serves as the primary thermosensory neurons required for thermotaxis (movement toward the a preferred temperature) [34]. The dendritic endings of AFD, enriched with microvilli, serve as the primary site for thermal detection. Even when detached from the cell body, these dendritic endings retain calcium responsiveness to temperature stimuli [35]. Moreover, genetically disrupting these sensory endings abolishes the Ca^{2+}

70 response in AFD cell bodies to temperature changes and eliminates thermotaxis, underscoring their
71 essential role in thermal sensing [36–38].
72 The second messenger cyclic guanosine monophosphate (cGMP) plays a central role in
73 modulating AFD thermosensory activity. Temperature changes in AFD neurons trigger intracellular
74 Ca^{2+} dynamics, with Ca^{2+} levels rising during warming and falling during cooling [35,39,40]. This
75 response relies on cGMP synthesis mediated by the guanylyl cyclases (GCs) *gcy-8*, *gcy-18*, and *gcy-*
76 *23*, which have overlapping but distinct roles. Specifically, *gcy-8* is essential for generating thermally
77 evoked Ca^{2+} responses in AFD [41,42], whereas *gcy-18* and *gcy-23* act synergistically to sustain
78 temperature sensing [41,43]. The cGMP produced by these cyclases activates cyclic nucleotide-
79 gated (CNG) channels, comprised of alpha-subunits TAX-4 and beta-subunits TAX-2, resulting in
80 increases in intracellular Ca^{2+}. Mutations in either *tax-4* or *tax-2* abolish thermally evoked Ca^{2+}
81 responses in AFD and disrupt thermotaxis, underscoring the importance of cGMP signaling for AFD-
82 mediated thermosensation [40].
83 AFD transmits thermal signals to several downstream interneurons, including AIY, AIZ, and AIB,
84 which process this information to guide temperature-dependent behaviors. Thermotaxis in *C.*
85 *elegans* encompasses three categories: movement toward warmer temperatures (thermophilic),
86 movement toward cooler temperatures (cryophilic), and movement within a preferred temperature
87 range (isothermal) [44,45]. Each behavior type depends on distinct AFD synaptic partners: AIY is
88 critical for thermophilic and isothermal behaviors [46,47]; AIZ is specific for cryophilic behavior [48–
89 50]; and AIB also supports thermophilic behavior, though its role is less critical than that of AIY [51].
90 These findings demonstrate the functional specificity of synaptic partners of AFD neurons in shaping
91 distinct temperature-dependent behaviors.
92 In this study, we demonstrate that AFD plays a novel role in tactile-mediated, context-dependent
93 locomotion modulation, thereby expanding its function beyond temperature sensing. The mechanisms
94 underlying this role differ markedly from those involved in thermosensation. First, context-dependent
95 modulation requires distinct cGMP signaling components. Second, while the microvilli-rich sensory

96 endings of AFD are essential for thermosensation, they are dispensable for context-dependent
97 modulation. Third, this modulation depends on mechanosensory neurons and on electrical synapses
98 between AFD and the AIB interneuron, which connects to mechanosensory circuits. Finally,
99 disruption of *inx-7* and *inx-10* genes, encoding gap junction protein innexins in AFD and AIB, impairs
100 context-dependent locomotion modulation. Remarkably, restoring AFD-AIB connectivity via
101 engineered Cx36 electrical synapses rescues this function. Collectively, our findings uncover an
102 unconventional mechanism by which AFD mediates behavior modulation based on tactile experience.
103

104 **RESULTS**

105

106 ***C. elegans* display distinct locomotion in identical environments after exploring different**
107 **physical structures.**

108 To test whether prior physical experience influences *C. elegans* behavior, we allowed worms to
109 explore microfluidic chambers with distinct pillar designs before recording their locomotion in identical
110 assay zones (Fig. 1A). Because the environment within the assay zone is the same across chambers,
111 behavioral differences observed there are likely to reflect an influence of prior tactile experience. To
112 implement this assay, we designed two microfluidic chambers that differ only in the physical structure
113 of the exploration zone: a uniform chamber and a binary chamber (Fig. 1A). Before reaching the
114 assay zone, worms explore surrounding areas with pillar designs that differ in size and spacing
115 (exploration zone, Fig. 1A). This design allowed us to assess how exposure to different physical
116 contexts impacts locomotion in an otherwise identical setting.

117 Worms were allowed to explore the chambers for 60 minutes before behavior was recorded in
118 the assay zones. We found that worms in the uniform chamber assay zone exhibited locomotor
119 behavior distinct from those in the binary chamber assay zone (Fig.1 B-F). Specifically, worms in the
120 uniform chamber assay zone moved approximately 40% faster (Fig. 1B, F), spent ~20% less time idle
121 (Fig. 1C, F), reversed direction ~20% less frequently (Fig. 1D, F), and turned ~30% more often (Fig.

122 1E, F) than worms in the binary chamber assay zone. Among the parameters measured, locomotion
123 speed showed the most robust and reproducible modulation, establishing a stable behavioral metric
124 for dissecting the underlying circuit and molecular mechanisms. These findings demonstrate that
125 locomotion is shaped by past sensory experience rather than solely by immediate environmental
126 cues.

127 Because worms in the binary chamber are exposed to both pillar types and remain free to
128 move between exploration and assay zones, the behavioral differences described above could reflect
129 exposure to a more complex physical environment rather than prior experience alone. To directly test
130 whether locomotion is modulated by prior physical experience independently of continued access to
131 the exploration zone, we designed microfluidic chambers in which the assay zone could be separated
132 from the exploration zone by a removable barrier (Fig. 1–Supplement 1A). In these chambers, worms
133 were initially allowed to explore the entire device, including exploration zones that either matched or
134 differed from the assay zone. A barrier was then inserted to prevent worms in the assay zone from re-
135 entering the exploration zones.

136 Under these conditions, locomotion immediately after barrier insertion was higher in worms
137 that had previously explored physical settings matching the assay zone (205 ± 8 μm/s) than in worms
138 that had explored non-matching settings (151 ± 7 μm/s; $p = 0.006$; Fig. 1–Supplement 1B). This
139 difference persisted when worms were recorded 40 minutes after barrier insertion, with animals in
140 matching chamber retaining their higher locomotion rates (218 ± 11 μm/s) compared to those in
141 non-matching chambers (185 ± 8 μm/s; $p = 0.02$; Fig. 1–Supplement 1B). These findings demonstrate
142 that prior exploration of distinct physical environments can modulate locomotion even when worms
143 are prevented from returning to those environments, supporting a role for prior physical experience
144 independent of ongoing sensory input.

145

146 **Guanylyl cyclase gene *gcy-18* is required for context-dependent locomotion modulation in**
147 **chambers.**

148 To identify mechanisms underlying context-dependent locomotion adjustments, we employed a
149 previously reported preference assay that uses microfluidic arenas to assess the ability of worms to
150 select a preferred space [52]. Because worms must adjust their locomotion based on their
151 surroundings to remain within a preferred area, we hypothesized that mutations abolishing this
152 preference would reveal key mechanisms underlying context-dependent adjustments in the uniform
153 and binary chambers. Accordingly, we screened for mutant worms that failed to choose their
154 preferred area, aiming to identify the genetic mechanisms mediating locomotion adjustments in
155 response to different physical structures.

156 Given the significant role of cGMP in neuronal plasticity and behavior modulation, we performed
157 a small-scale genetic screen using loss-of-function mutants for 24 genes encoding guanylyl cyclases
158 (GCs), the enzymes responsible for cGMP synthesis. Using the preference assay, we identified two
159 putative null mutants, *gcy-18(gk423024)* and *gcy-12(gk142661),* that displayed significant defects in
160 spatial preference (Fig. 2–Supplement 1A). We then compared the locomotion of *gcy-18* and *gcy-12*
161 mutants in both uniform and binary chambers. *gcy-12* mutant worms exhibited normal speed
162 adjustment compared to wild type (Δspeed: *gcy-12*: 24 ± 5% vs. N2: 35 ± 7%, p = 0.27, Fig. 2–
163 Supplement 1B), indicating that *gcy-12* is not required for locomotion modulation. In contrast, *gcy-*
164 *18(gk423024)* mutants failed to execute context-dependent speed adjustment (Δspeed *gcy-18*: 3 ±
165 5% vs. N2: 35 ± 7%; p = 0.0013; Fig. 2A). A second allele, *gcy-18(nj38),* similarly showed significantly
166 reduced Δspeed (11 ± 2%; p =0.011 compared to wild type; Fig. 2A). Together, these results indicate
167 that *gcy-18* is required for context-dependent behavioral adjustment.

168 To confirm that the defects observed in *gcy-18* mutants were not due to background artifacts, we
169 introduced a single-copy *gcy-18* transgene driven by the *gcy-18* promoter into *gcy-*
170 *18(gk423024)* mutants. Expression of this transgene restored locomotion adjustments to near wild
171 type levels (Δspeed: *gcy-18p::gcy-18*: 28 ± 6% vs. N2: 35 ± 7%, p = 0.8, Fig. 2B), confirming that loss
172 of *gcy-18* underlies the observed behavioral defects. The identification of *gcy-18* was particularly
173 intriguing, as its expression is restricted to a single pair of neurons, the thermosensory AFDs. Given

174 that our assay chambers lacked thermal gradients, these findings suggest a previously unrecognized
175 role for *gcy-18* and AFD neurons in mediating locomotion adjustments based on prior exploration of
176 physical environments.

177 To further investigate the role of AFD-specific guanylyl cyclases in context-dependent
178 locomotion modulation, we examined *gcy-8*, which is essential for generating thermally evoked Ca^{2+}
179 responses in AFD [41,42]. In thermal responses, disrupting *gcy-8* alone is sufficient to impair AFD
180 function, whereas disruption of *gcy-18* alone does not [41,43], indicating the critical role of GCY-8 in
181 AFD thermosensation. If *gcy-18* influenced behavioral adjustment in microfluidic chambers solely
182 through its role in thermosensation, we would expect that a loss-of-function mutation in *gcy-8* would
183 have a similar or even more disruptive impact on locomotion modulation. However, *gcy-8* mutant
184 worms exhibit little change in their ability to adjust locomotion speed, with Δspeed values similar to
185 that observed in wild type worms (Δspeed: *gcy-8*: 29 $\pm$ 7% vs. N2: 35 $\pm$ 7%; $p = 0.96$; Fig. 2C). These
186 results indicate that while *gcy-8* is critical for thermosensation, its mutation does not affect context-
187 dependent locomotion modulation, suggesting that independent cGMP signaling mechanisms govern
188 AFD neuronal activity in thermosensation and context-dependent behavior in microfluidic chambers
189 (Fig. 2D).

190

191 **Distinct CNG channels mediate context-dependent locomotion modulation and**
192 **thermosensation.**

193 The role of guanylyl cyclase in cGMP synthesis prompted us to investigate whether cyclic
194 nucleotide-gated (CNG) channels are involved in context-dependent locomotion modulation. CNG
195 channels, composed of α and β subunits, open upon binding cyclic nucleotides (*e.g.*, cGMP and
196 cAMP), allowing Ca^{2+} influx [53–56] to control signal transduction and neural plasticity across species
197 [57–64] (Fig. 3A). In *C. elegans*, mutations in either the *tax-4* or *tax-2* genes, which encode the α and
198 β subunits of CNG channels respectively, impair thermotaxis behavior [47,65] and eliminates AFD
199 responses to temperature changes [40,66]. To determine their role in context-dependent locomotion

200 modulation, we examined *tax-4(p678)* and *tax-2(p694)* mutant worms using our microfluidic chamber
201 assay.

202 We found that *tax*-2 is essential for context-dependent locomotion modulation, as *tax-2* mutants
203 did not exhibit differences in speed between chamber types (Fig. 3B, C). In contrast, *tax-4* mutants
204 displayed an enhanced locomotion adjustment compared to wild type worms (Δspeed: *tax-4*: 68 ± 6%
205 vs. N2: 41± 6%; p = 0.002; Fig. 3C), a striking difference from the lack of speed changes seen in *tax-*
206 *2* mutants (Δspeed: *tax-2*: 2 ± 2%; p < 0.0001 compared to wild type). We examined the locomotion
207 speed of mutant worms in the binary chambers, which we refer to as the basal speed because wild
208 type worms consistently move slowest in this environment. We found *tax-4* mutants showed
209 significantly higher basal speed than the wild type (*tax-4:* 193 ± 9 μm/s vs. N2: 104 ± 4 μm/s, p <
210 0.0001; Fig. 3B), indicating that *tax-4* mutants can still adjust locomotion speed based on prior
211 experience even when basal locomotion is accelerated.

212 To further examine how basal locomotion influences context-dependent modulation, we took
213 advantage of the fact that worm locomotion rates are sensitive to environmental temperature [67,68].
214 We examined the relationship between temperature-induced changes in basal locomotion and
215 locomotion modulation based on prior experience of physical surroundings. Wild type worms
216 cultivated at either 23°C or 17°C and then transferred to 20°C exhibited significantly changes in basal
217 locomotion speed. Despite changes in basal speed, the extent of locomotion modulation in the
218 chambers was largely unaffected (Fig.3–Supplement 1A). Specifically, locomotion speed was
219 positively correlated with temperature shifts in both chambers (binary chambers: r = 0.52, p < 0.0001;
220 uniform chambers: r = 0.48, p < 0.0001; Fig.3–Supplement 1B), whereas no significant correlation
221 was observed between temperature and Δspeed (r = -0.03, p = 0.22; Fig.3—Supplement 1C),
222 supporting the notion that basal locomotion speed and context-dependent modulation are regulated
223 independently.

224 Together, these observations indicate that TAX-2 is required for integrating prior experience into
225 locomotion modulation, whereas TAX-4 primarily regulates overall locomotion level. Although both

226 pathways engaging cGMP signaling, their distinct phenotypes suggest separate regulatory
227 mechanisms for basal locomotion and context-dependent adjustments.

228 Given that four other genes (*cng-1, cng-2, cng-3* and *cng-4*) are predicted to encode CNG
229 channels in *C. elegans,* we investigated their role in locomotion modulation in microfluidic chambers
230 [69]. Due to abnormal development in *cng-1* mutants, we were unable to assess their locomotion;
231 however, we were able to evaluate mutants of the other three genes. We found that *cng-*
232 *3(gk541751)* mutant worms showed significantly decreased speed modulation compared to wild type
233 (Δspeed: *cng-3:* 5 ± 4%, p = 0.0002; Fig. 3D), while *cng-2(tm4267)* and *cng-4(gk195496)* mutants
234 exhibited normal modulation comparable to wild type worms (p = 0.54 and p = 4.47 respectively; Fig.
235 3D). The identification of CNG-3 was particularly intriguing, as recent studies suggest that it mediates
236 changes in AFD neuronal activity based on prior temperature experiences [70,71], indicating that
237 CNG-3 contributes to neural plasticity rather than direct stimulus detection. Our results further support
238 this view by showing that CNG-3 plays a broader role in locomotion modulation in environments
239 lacking thermal gradients, which suggests its involvement in neuronal plasticity beyond the
240 thermosensory modality.

241 Next, we determined whether AFD is the site where CNG-3 functions in context-dependent
242 locomotion modulation. To do so, we introduced single-copy transgenes expressing *cng-3* cDNA
243 under the control of two AFD-specific promoters, *srtx-1Bp* and *gcy-18p*, into *cng-3(gk541751)* mutant
244 worms. Regardless of the promoter used, AFD-specific expression of *cng-3* restored the locomotion
245 speed modulation to levels comparable to wild type (Δspeed: *srx-1Bp::cng-3*: 47 ± 8%; p < 0.0001
246 compared to *cng-3* mutant, p = 0.91 compared to wild type; and *gcy-18p::cng-3:* 40 ± 6%, p = 0.0007
247 compared to *cng-3* mutant, p = 0.99 compared to wild type; Fig. 3E). These results indicate that AFD
248 neurons are the site of action for CNG-3 in mediating context-dependent locomotion modulation.
249 Together, our findings reveal a role for AFD beyond thermosensation and show that components of a
250 cGMP signaling pathway enable AFD to modulate locomotion in an experience-dependent manner.
251

252 **AFD sensory microvilli are dispensable for locomotion modulation, but AFD neurons are**
253 **required.**
254 The finding that GCY-18 and CNG-3 in AFD neurons are required for context-dependent
255 locomotion prompted us to test whether the AFD thermosensory apparatus is also necessary for this
256 function. This apparatus consists of sensory microvilli at the tip of the AFD dendrite (Fig. 4A) and is
257 essential for temperature sensing and thermotaxis [36,38]. For example, mutations in the *kcc-3* gene,
258 which encodes a K^+/Cl^- cotransporter in the amphid sheath glia, disrupt microvilli formation and
259 significantly impair thermotaxis toward the cultivation temperature [37].
260 Despite this disruption, locomotion modulation based on experience of physical settings
261 remained intact in *kcc-3(ok228)* mutant worms compared to wild type (Δspeed: *kcc-3*: 33 ± 4% vs.
262 N2: 42 ± 7%, p = 0.28; Fig. 4B, C). *kcc-3* mutants also displayed elevated basal locomotion rates
263 (basal speed: *kcc-3:* 174 ± 8 μm/s vs. N2: 115 ± 7 μm/s, p < 0.0001; Fig. 4B), similar to what we
264 observed in *tax-4* mutants. This supports our earlier finding that overall locomotion rate does not
265 necessarily correlate with context-dependent modulation.
266 To further test whether AFD sensory endings are required for context-dependent locomotion
267 modulation, we examined *ttx-1(767)* mutant worms, which completely lack AFD microvilli and exhibit
268 more severe thermotaxis defects than *kcc-3* mutants [38]. Despite the loss of sensory microvilli, *ttx-1*
269 mutants retained the ability to modulate locomotion in microfluidic chambers. The extent of
270 modulation was modestly reduced and more variable compared to wild type animals (Δspeed: *ttx-1*:
271 29 ± 10% vs. N2: 42 ± 7%, p = 0.29, Fig. 4D). Because *ttx-1* mutations disrupt the expression of
272 multiple AFD genes, including components of the cGMP signaling pathway [72], this increased
273 variability may reflect broader perturbations in AFD function. Nonetheless, these results indicate that
274 AFD sensory microvilli are not strictly required for context-dependent locomotion modulation.
275 Given that *gcy-18* is required for context-dependent locomotion modulation and that GCY-18
276 localizes to the distal dendrite of AFD, we next examined how disruption of sensory microvilli affects
277 its localization in AFD. We used a split-GFP strategy to visualize endogenous GCY-18 [73]. A tandem

278 array of seven GFP11 β-strands (GFP11x7) was inserted at the C-terminus of GCY-18 using
279 CRISPR-Cas9. When complemented with GFP1-10, GCY-18::GFP11x7 fluorescence was strongly
280 enriched at the AFD sensory microvilli near the nose (Fig. 4–Supplement 1A-A″), consistent with
281 previous reports [42,74,75]. In addition, weaker but reproducible GCY-18 signal was detected near
282 the AFD soma and axon (Fig. 4–Supplement 1A‴). Importantly, in *kcc-3*, which exhibit disrupted
283 sensory microvilli, and *ttx-1* mutants, which lack sensory microvilli, GCY-18 remained localized to the
284 distal dendrite and was still detectable near the soma and axon (Fig. 4–Supplement 1B-B‴ and 1C-
285 C‴). Although these experiments do not identify the precise subcellular site at which GCY-18 acts,
286 they show that disruption or loss of sensory microvilli does not substantially alter GCY-18 localization
287 within AFD.

288 We next asked whether AFD neurons themselves are required for this behavior. Using a
289 published strain expressing caspase under the AFD-specific *gcy-8* promoter [76], we found that AFD-
290 ablated worms completely lost the ability to adjust locomotion in microfluidic chambers. These
291 animals showed no detectable differences between uniform and binary chambers in locomotion
292 speed, idle time, or turning frequency (Fig. 4E). Together, these results indicate that while AFD
293 sensory microvilli are dispensable for context-dependent locomotion modulation, the AFD neurons
294 themselves are essential.

295 Building on our finding that locomotion modulation can be driven by prior physical experience
296 even after worms are prevented from re-entering the exploration zones, we next tested whether AFD
297 is required for this modulation using chambers in which the exploration and assay zones were
298 separated by a removable barrier (Fig. 1–Supplement 1A). Under these conditions, locomotion
299 modulation was significantly reduced in AFD-ablated worms (Δspeed: -AFD = 1 ± 6% vs. N2 =
300 23 ± 7%; p = 0.036; Fig. 4–Supplement 2A). Similarly, *gcy-18* mutants showed defective locomotion
301 modulation (Δspeed: *gcy-18* = -1 ± 8% vs. N2 = 23 ± 7%; p = 0.034; Fig. 4–Supplement 2A). These
302 results indicate that AFD and *gcy-18* are required to generate locomotion modulation in response to
303 recent physical experience.

304 Finally, to determine whether the modulation defects observed in *gcy-18* mutants and AFD-
305 ablated worms could be attributed to developmental abnormalities or gross motor impairments, we
306 measured locomotion speed and body length on standard NGM plates. Both day-1 adult AFD-ablated
307 worms (speed: 281 ± 10 μm/s; p = 0.33; body length: 1.12 ± 0.01 mm; p = 0.76) and *gcy-18* mutants
308 (speed: 291 ± 13 μm/s; p = 0.22; body length: 1.15 ± 0.02 mm; p = 0.86) showed locomotion speeds
309 and body lengths comparable to wild type controls (speed: 252 ± 30 μm/s; body length: 1.14 ± 0.02
310 mm; Fig. 4–Supplement 2B, C). These results indicate that the loss of context-dependent locomotion
311 modulation is not due to developmental defects or gross impairments in locomotion.
312

313 **Context-dependent locomotion modulation requires the MEC-10 mechanosensory channel**
314 **subunit.**

315 Having established that AFD integrates prior physical experience independent of its
316 thermosensory apparatus, we next asked whether direct mechanosensory input is required for
317 context-dependent locomotion modulation. The *mec-10* gene encodes an amiloride-sensitive Na^+
318 channel protein required for sensing body touch. Mutations in *mec-10* disrupt mechanotransduction
319 channels in the worms, impairing touch sensitivity [77,78]. We found that *mec-10(tm1552)* mutants
320 failed to display locomotion adjustment compared to wild type worms (Δspeed: *mec-10*: 5 ± 4% vs.
321 N2: 33 ± 6%, p = 0.0003; Fig. 5A). These results show that *mec-10* is crucial for context-dependent
322 locomotion modulation, supporting the hypothesis that locomotion is modulated depending on the
323 worm's tactile experience.

324 The *mec-10* gene is expressed in several mechanosensory neurons, including the six touch
325 receptor neurons (TRNs) and the polymodal nociceptors FLP and PVD [77,79]. To determine which
326 neurons are required for tactile-dependent locomotion modulation, we expressed *mec-10* cDNA
327 under cell-specific promoters: *mec-18p* (TRNs) [80], *egl-44p* (FLP) [81], or *mec-10p* (TRNs, FLP, and
328 PVD) [79]. Expression in either FLP or TRNs alone did not restore modulation, as worms carrying *egl-*
329 *44p::mec-10* (Δspeed: -11 ± 4%) or *mec-18p::mec-10* (Δspeed: -13 ± 4%) transgenes showed

330 significantly reduced Δspeed compared to wild type (Δspeed: N2: 33 ± 6%; $p < 0.0001$ for both; Fig.
331 5A). By contrast, *mec-10* co-expression in both FLP and TRNs (Δspeed: 16 ± 4%), or expression
332 from the *mec-10* promoter (Δspeed: 23 ± 4%), restored Δspeed to wild type levels ($p = 0.20$ and $p =$
333 0.57, respectively; Fig. 5A). These findings indicate that *mec-10* expression across multiple
334 mechanosensory neuron types is required for context-dependent locomotion modulation. It is also
335 worth noting that, while both tactile-dependent locomotion modulation and previously reported spatial
336 preference require FLP, only the former depends on TRNs. Together, these findings suggest that
337 distinct subsets of mechanosensory neurons differentially contribute to behaviors shaped by tactile
338 experience.
339
340 **AIB interneurons are crucial for tactile-dependent behavioral plasticity.**
341 Touch-sensitive neurons that express *mec-10*, including TRNs, FLP, and PVD, do not form
342 direct synapses with AFD, suggesting that tactile information is relayed through intermediary neurons.
343 Because the interneuron AIB receives synaptic input from FLP and forms electrical synapses with
344 AFD, we hypothesized that AIB could serve as a conduit for mechanosensory signals to reach AFD.
345 To test whether AIB is required for tactile-dependent modulation, we examined locomotion in worms
346 with genetically ablated AIB neurons using *npr-9p::caspase* expression [82]. AIB-ablated worms failed
347 to adjust locomotion speed, showing a near-complete loss of modulation (Δspeed: -1 ± 5%) compared
348 to wild type (30 ± 8%, $p = 0.001$, Fig. 5B). These results demonstrate that AIB is required for AFD-
349 mediated tactile-dependent locomotion modulation. However, because *mec-10*-expressing TRNs are
350 also required, additional pathways beyond AIB likely contribute to transmitting tactile information to
351 AFD, potentially involving indirect synaptic connections through other interneurons or long-distance
352 signaling via neuropeptides or other modulators (Fig. 5C).
353
354 **Mutations in *innexin* genes disrupt tactile-dependent modulation.**

355 Electrical synapses between AIB and AFD neurons in *C. elegans* are formed by gap junction
356 proteins known as innexins [83]. If electrical coupling between AIB and AFD contributes to tactile-
357 dependent locomotion modulation, then disruption of innexin genes should impair locomotion
358 adjustments in microfluidic chambers. To test this, we examined loss-of-function mutants of several
359 innexin genes. *C. elegans* possesses 25 innexin genes [84,85]. Single-cell RNA-seq data from the
360 CeNGEN database [86] indicate that three genes (*inx-4, inx-10,* and *inx-19)* are expressed in AFD*,*
361 one (*inx-1)* is expressed in AIB, and one (*inx-7*) is expressed in both*.* We found that *inx-4, inx-7*, and
362 *inx-10* mutants exhibited a partial but significant reduction in locomotion modulation compared to wild
363 type worms (Δspeed: N2: 45 ± 7%; *inx-4*: 23 ± 5%, p = 0.037; *inx-7*: 21 ± 5%, p = 0.013; *inx-10*:
364 16 ± 3%, p = 0.0007; Fig. 6A). Mutations in *inx-1* also reduced Δspeed values, although the effect did
365 not reach statistical significance (Δspeed: *inx-1:* 25 ± 6%, p = 0.076), whereas *inx-19* mutations had
366 little impact on speed modulation (*inx-19:* 32 ± 5%, p = 0.51, vs. wild type; Fig. 6A). Furthermore, *inx-*
367 *7; inx-10* double mutants exhibited a more pronounced reduction in Δspeed compared to single
368 mutants (Δspeed: *inx-7; inx-10* double mutant: 6 ± 5%; p = 0.032 compared to *inx-7* single mutant;
369 Fig. 6B). Together, these findings suggest that multiple innexin genes act redundantly to support
370 tactile-dependent locomotion modulation.
371
372 **Targeted electrical coupling between AFD and AIB restores tactile-dependent modulation.**
373 We next tested whether restoring *inx-10* specifically in AFD would be sufficient to rescue the
374 behavioral defect. Using the AFD-specific *srtx-1b* promoter, we expressed *inx-10* cDNA in *inx-10*
375 mutant worms. These transgenic animals displayed significantly improved locomotion modulation
376 (Δspeed: 42 ± 5%) compared to non-transgenic *inx-10* mutants (15 ± 4%; p = 0.018; Fig. 6D),
377 indicating that *inx-10* expression in AFD alone is sufficient to restore function.
378 To directly test whether restoring the electrical connection between AFD and AIB could rescue
379 modulation in innexin mutants, we expressed the mammalian gap junction protein Cx36 [87–90] in
380 both AFD (*srtx-1Bp*) and AIB (*inx-1p*) neurons in *inx-7; inx-10* double mutants (Fig. 6C). Cx36

381 expression significantly improved locomotion modulation, restoring Δspeed from 7 ± 4% to 35 ± 8% (p
382 = 0.0035; Fig. 6D). These results demonstrate that although innexin mutations disrupt connectivity
383 across multiple neurons, restoring a single targeted electrical connection between AFD and AIB is
384 sufficient to rescue tactile-dependent locomotion modulation, identifying the AIB-AFD electrical
385 synapse as a critical circuit element for tactile-dependent behavioral control.
386
387 **DISCUSSION**
388
389 Our study reveals that the thermosensory AFD neuron plays an unexpected role in coupling tactile
390 experiences to locomotion modulation in *C. elegans*. We show that: 1) *C. elegans* exhibit distinct
391 locomotion patterns in identical environments, influenced by prior tactile experiences; 2) tactile-
392 dependent behavior modulation requires the AFD neuron but not its thermosensory dendritic endings;
393 3) thermotaxis and tactile-dependent locomotion modulation rely on distinct sets of cGMP signaling
394 proteins and CNG channel subunits; 4) the AIB interneuron, which connects AFD to mechanosensory
395 circuits, is essential for tactile modulation; and 5) electrical synapses between AFD and AIB are
396 critical for this process. Below, we discuss the implications of these findings.
397
398 **A thermosensation-independent role for AFD in tactile-dependent behavior modulation.**
399 Our findings highlight the remarkable versatility of sensory neurons in shaping behaviors beyond
400 their primary functions. This supports the emerging view that sensory neurons have multifaceted roles
401 in circuit modulation, extending well beyond canonical sensory activities. Such complexity is encoded
402 at multiple levels within neural circuits. In *C. elegans*, for instance, the ASH neuron drives avoidance
403 responses to various noxious stimuli, including hyperosmolarity, nose touch, and volatile repellents,
404 demonstrating polymodal functionality [91–94]. Similarly, the olfactory receptor neuron AWC exhibits
405 stochastic responses to temperature, introducing variability that enhances the flexibility and reliability
406 of thermotactic behavior [95–97]. In contrast to these examples, the role of AFD in tactile-dependent

407 plasticity does not rely on its sensory endings but is mediated through synaptic connectivity. This
408 reveals an unexpected mechanism by which AFD influences context-dependent behavioral plasticity
409 via network-level interactions rather than direct sensory activity.
410

411 **Distinct cGMP signaling pathways in AFD mediate sensation and plasticity.**

412 Our data indicates that the CNG channel α subunits TAX-4 and CNG-3 play distinct roles in AFD
413 function. Although TAX-4 is essential for AFD to detect temperature and generate thermally evoked
414 responses [40], it is dispensable for tactile-dependent locomotion modulation. By contrast, CNG-3,
415 which is not required for temperature sensing [70], is crucial for tactile-dependent locomotion
416 modulation. Consistent with a broader role in sensory plasticity, CNG-3 is required in AWC neurons
417 for short-term odor adaptation [98] and in AFD for adjusting temperature thresholds based on prior
418 thermal experiences [70]. Our demonstration that CNG-3 is essential for tactile-dependent locomotion
419 modulation further supports the view that CNG-3 enables context-dependent behavioral plasticity
420 rather than directly mediating stimulus detection.

421 CNG channels are heteromeric complexes composed of both α and β subunits. Our data, along
422 with previous work, show that TAX-2, the CNG β subunit in *C. elegans*, is required for both tactile-
423 dependent locomotion modulation and thermotransduction [40]. Interestingly, TAX-4, the canonical α
424 partner of TAX-2, is not required for tactile-dependent modulation. This suggests that TAX-2 may
425 support experience-dependent neural plasticity either on its own or by pairing with alternative α
426 subunits such as CNG-3. This type of functional specialization is reminiscent of photoreceptor
427 neurons, where the composition and ratio of CNG channel subunits determine light sensitivity and
428 enable contrast detection under varying light intensities [99–101]. It is worth noting that the *tax-*
429 *2(p694)* mutation affects *tax-2* expression in four neurons (AFD, BAG, ASE, and ADE) [102].
430 Moreover, the strong convergence of functional and circuit-level evidence, including the requirement
431 for GCY-18, the rescue of CNG-3 function in AFD, and role of AIB–AFD coupling, points to AFD as
432 the most likely site of TAX-2 function in tactile-dependent locomotion modulation.

433 In addition to the diversity of CNG channels, guanylyl cyclases in AFD also exhibit functional
434 specificity. For example, mutations in *gcy-18* alone significantly disrupt tactile-dependent locomotion
435 modulation without substantially affecting temperature sensing [41,43], whereas *gcy-8* is essential for
436 generating thermally evoked Ca^{2+} responses [41,42] yet appears dispensable for tactile-dependent
437 plasticity. These results show that AFD uses distinct sets of guanylyl cyclases to execute dual roles:
438 precise temperature sensing and tactile-dependent behavioral modulation.
439
440 **Differential regulation of context-dependent plasticity and basal locomotion rates in AFD.**
441 Our results further suggest that the mechanisms controlling basal locomotion and context-
442 dependent behavioral modulation are not only distinct but also operate independently. Temperature
443 fluctuations significantly affect basal locomotion rates, i.e., higher temperatures accelerate speed,
444 while lower temperatures slow it down [67,68]. However, tactile-dependent locomotion modulation in
445 microfluidic chambers remains robust despite these temperature-induced changes in basal
446 movement. This independence is further supported by our observations in *tax-4* and *kcc-3* mutants,
447 which display elevated basal locomotion rates yet still adjust their locomotion in response to tactile
448 experiences. These findings indicate that the processes governing basal locomotion and context-
449 dependent modulation are controlled by separate, non-interfering mechanisms, even though both
450 pathways engage cGMP signaling.
451
452 **Electrical synapses link the thermosensory neuron AFD to tactile-dependent behavioral**
453 **modulation.**
454 AIB-AFD electrical synapses are pivotal for tactile-dependent behavioral plasticity. Disrupting
455 this connection impairs tactile-dependent locomotion modulation, whereas restoring an engineered
456 electrical synapse rescues this behavior. The successful replacement of invertebrate innexins with
457 vertebrate connexins, which perform analogous functions despite lacking sequence homology,
458 indicates that the core function of these synapses lies in their connectivity rather than in their specific

459 protein sequences. This observation suggests that the transfer of signaling molecules such as Ca^{2+}
460 and cGMP through electrical synapses may facilitate the coordination of neuronal activity across
461 distinct networks [103–106].

462 Together, these findings support a model in which AIB functions as a hub neuron that relays
463 mechanosensory input from FLP to AFD to modulate locomotion (Fig. 5C). However, because
464 electrical synapses are often bidirectional, information flow may also occur in the opposite direction,
465 from AFD to AIB. Determining the directionality and dynamics of this signaling remains an important
466 question for future investigation. A similar circuit logic has been proposed for thermal avoidance
467 behavior, in which AIB integrates inputs from FLP via chemical synapses and couples to AFD via
468 electrical synapses, forming an FLP-AIB-AFD circuit. In that case, the directionality of information flow
469 also remains unresolved [107].

470 Finally, the proposed circuit mechanism for tactile-dependent modulation does not exclude
471 additional routes of modulation. These may include extra-synaptic signaling mechanisms, such as
472 neuropeptide release from other touch-sensitive neurons. While the precise molecular and circuit
473 mechanisms remain to be elucidated, our findings establish that AIB-AFD electrical synapses are
474 essential for incorporating tactile context into locomotor control.

475

476 **IN SUMMARY**, our findings reveal an unexpected role for AFD in tactile-dependent behavioral
477 plasticity. They show that specialized molecular mechanisms, including distinct cGMP signaling
478 pathways, diverse guanylyl cyclases, and functional electrical synapse connectivity, enable AFD
479 sensory neurons to perform dual functions: detect stimuli and support tactile-dependent plasticity. A
480 limitation of this study is that the directionality and mode of information flow between AFD and AIB
481 remain unresolved, and defining this relationship will be an important goal for future investigation.
482 Nevertheless, our results establish the AFD-AIB connection as a regulatory hub in tactile-dependent
483 locomotor modulation and expand our understanding of sensory neuron versatility in adaptive
484 behavior.

ACKNOWLEDGEMENTS. This research was supported by NIH grants R01NS109476 and R01NS115974 to JB. MR was supported by T32GM136534 and F31NS129545. The authors thank the Caenorhabditis elegans Genetics Center (funded by the NIH Office of Research Infrastructure Programs P40 OD010440) for providing worm strains. We also thank Lin Zhang and Yan Liu for their support in constructing DNA plasmids and generating transgenic worm strains. Special thanks to Melissa Woo (Mercer Island High School), Tabitha Ngo, and Sahithi Challam (Interlake High School) for their assistance with worm maintenance. We appreciate the members of the Bai lab for their critical reading of the manuscript. Additionally, we acknowledge the multiple mentorship programs at Fred Hutchinson Cancer Center, including the SURP Undergraduate Researchers and Pathways Undergraduate Researchers programs, supported in part by the Cancer Center Support Grant P30 CA015704, for fostering relationships with high school and undergraduate trainees who contributed to this project.

METHODS

Nematode Strains and Growth – *C. elegans* strains were maintained under standard conditions at 20°C on nematode growth medium (NGM) agar plates [108]. These plates were seeded with *E. coli* OP50 lawns. Strains used in this study are listed in Table S1 and are available from the corresponding author upon request.

Molecular Biology – All DNA constructs were sequence-verified. cDNA sequences encoding *mec-10*, *cng-3*, and *inx-10* were amplified from a cDNA library made with the SuperScript III Reverse Transcriptase kit (Thermo Fisher Scientific, MA) from total RNA extracted from adult N2 worms. A codon-optimized cDNA sequence for the mouse gap junction protein connexin-36 (Cx36) was previously described [109]. DNA plasmid constructs for *C. elegans* expression were assembled by LR

511 recombination using the MultiSite Gateway Three-Fragment Vector Construction Kit (Thermo Fisher
512 Scientific, MA). Entry clones were constructed as follows: (i) promoter sequences flanked by attL4
513 and attR1 sites; (ii) cDNA sequences flanked by attL1 and attL2 sites; and (iii) *sl2::mNeonGreen::rab-*
514 *3 3'utr* flanked by attR2 and attL3 sites. Destination vectors used for LR recombination included the
515 pDEST R4-R3 Vector II and a custom-built destination vector BJP-C957, which contains a
516 hygromycin resistance cassette for selection, an intestinal fluorescent marker (*vha-6p::mScarlet::tbb-*
517 *2 3'utr*) for visual screening transgenic worms, and flanking *mos1* sequences to facilitate homologous
518 recombination for Mos1-mediated single-copy insertion (MosSCI). Promoters used for tissue- or cell-
519 specific expression were: *gcy-18p* (2 kb) and *srtx-1Bp* (493 bp) for AFD; *mec-18p* (390 bp) for TRNs;
520 *egl-44p* (5 kb) for FLP; *inx-1p* (1kb) for AIB, and *mec-10p* (3 kb) for expression in TRNs, FLP, and
521 PVD. Plasmids used to generate transgenic strains in this study are listed in Table S2.
522
523 **Transgenes, Germline Transformation, and Genome Editing –** Strains carrying extrachromosomal
524 arrays were generated by microinjecting various plasmids together with co-injection markers. The co-
525 injection markers included *unc-112p::gfp* (30 ng/µl), *rpl-28p::neoR* (20 ng/µl), and *Cbr-unc-119* (20
526 ng/µl). The blank vector pBluescript was used as filler DNA to bring the final total DNA concentration
527 to 100 ng/µl. A detailed list of the plasmids used to create transgenic worms in this study is provided
528 in Table S2.
529 Mos1-mediated transgene insertion [110,111] was used to generate single-copy transgenic
530 animals. Briefly, worms carrying the *ttTi5605 Mos1* site on chromosome II were injected with a
531 plasmid mixture containing the transgene of interest (40 ng/µl), along with BJP-B908, a plasmid
532 expressing Cas9 and a guide RNA targeting the Mos1 site (60 ng/µl). Selection markers included *rps-*
533 *0p::hygR* for hygromycin resistance and *vha-9p::mScarlet* for intestinal red fluorescence to enable
534 visual screening.
535 The *gcy-18::gfp11×7* knock-in strain was generated using a modified CRISPR–Cas9 protocol
536 employing preassembled Cas9 ribonucleoprotein (RNP) complexes, co-injected with a single-

537 stranded DNA repair template to facilitate homologous recombination [112,113]. Cas9 protein and
538 crRNA (targeting sequence: TACAACGACTGAAAGAGGAG) were obtained from Integrated DNA
539 Technologies (IDT, NJ). The single-stranded DNA repair template for generating *gcy-18::gfp11×7* was
540 synthesized by Twist Bioscience. Successful editing produced the *pek331* allele, which carries an in-
541 frame GFP11×7 insertion at the C-terminus of GCY-18. The insertion was verified by PCR and DNA
542 sequencing. A worm strain, BJH833, carrying both *pek331* and *muIs253 [eft-3p::sfgfp1-10::unc-54*
543 *3'utr],* was used to visualize GCY-18 by complemented split-GFP fluorescence [114].
544
545 **Fabrication of PDMS Microfluidic Chambers –** Microfluidic chamber designs were created in
546 AutoCAD and fabricated as 100 µm SU8-silicon molds using photolithography (FlowJem, NO,
547 Canada). PDMS devices were produced by pouring degassed PDMS prepolymer (Sylgard 184, Dow
548 Corning, MI) onto the molds, degassing again under vacuum (-25 inHg, 15 min, room temperature),
549 and curing at 80 °C for 2 hours. The cured PDMS was peeled from the mold, and inlet/outlet ports
550 were punched using a 2 mm biopsy punch (Acuderm Inc., FL). For the chambers with a removable
551 barrier shown in Figure 1–Supplement 1A, cast PDMS chamber structures were bonded onto a thin
552 semi-cured PDMS sheet to create a permanent, watertight seal. To prepare the sheet, ~30 ml of
553 PDMS was poured into a 6-inch Petri dish, degassed for 15 min, and partially cured at 65 °C for 15-
554 20 min, until firm but still tacky. PDMS chamber structures were gently placed onto the sheet with ~2
555 mm spacing to allow the formation of a barrier, then fully cured at 80 °C for 30 min. PDMS devices
556 were bonded to 1 mm glass microscope slides using oxygen plasma treatment (PDC-32G, Harrick
557 Scientific, NY, 1 min).
558
559 **Behavior Recording and Analysis –** Videos were captured for 10 seconds at 7.5 frames per second
560 using a Basler acA2440 camera (Basler, PA) equipped with an AF Micro-NIKKOR 60 mm lens
561 (Nikon, NY). Behavioral data were extracted from the videos using WormLab software (MBF
562 Bioscience, VT) through individual worm tracking. Only those worms that were already within the

563 assay area at the start of the recording were analyzed, and any worms that entered later were
564 excluded. Crawling speed was determined by the total distance traveled by a worm during the 10
565 second recordings. A turn was defined as a change in crawling direction of 15° or more. Reversals
566 were defined as sudden movement in the opposite direction for at least 5 frames (~0.6 seconds).
567 Worms were considered idle if their absolute velocity (distance traveled between frames) was below
568 20 μm/s for more than 10 frames (~1.3 seconds).

569 For behavior analysis, worms were age-synchronized by transferring 30-50 young adult worms
570 onto an NGM plate seeded with OP50 and allowing them to lay eggs for 2 hours before removal. The
571 plates were then kept at room temperature (22°C) for 3 days, allowing the eggs to develop into young
572 adults, identified by the presence of 5-10 eggs arranged in single rows within the gonads of all worms
573 on the plate. To wash the synchronized adults off the plate, worms were gently transferred into
574 Eppendorf tubes using glass Pasteur pipettes. After allowing the worms to settle at the bottom of the
575 tube (~1 minute), the supernatant was removed and replaced with fresh M9 buffer. This washing step
576 was repeated three times to remove residual OP50. Next, approximately 30-70 worms were loaded
577 into an inlet of the chambers shown in Figure 1 using a 20μl pipette and allowed to roam freely in the
578 chamber for 60 minutes before behavior in the assay area was recorded.

579 To assay worms confined to the assay area by a barrier (Fig. 1–Supplement 1A), PDMS
580 chambers were prepared with a removable gap separating the training and assay zones. M9 buffer
581 was first injected into the exploration zone, after which ~100 worms were loaded and allowed to
582 explore for 10 minutes, during which they moved only within the reach of the M9 buffer, typically up to
583 the gap between the exploration and assay zones. To remove the barrier, additional M9 buffer was
584 gently introduced into the assay zone until it merged with the buffer, allowing worms to move freely
585 between zones. After 15 minutes of exploration, the barrier was reintroduced by completely drying the
586 space between the zones with a Kimwipe, once again confining worms to areas containing M9 buffer.
587 Behavior in the assay zone was recorded immediately after the barrier was reinserted and again 40
588 minutes later.

589

590 **Fluorescence microscopy –** Widefield fluorescence microscopy was performed using a Leica DMi8
591 inverted microscope equipped with 63x/1.4NA and 100x/1.4NA oil-immersion objectives (Leica
592 Biosystems, NJ). Worms were mounted on thin 3% agar pads and anesthetized with 10 mM
593 levamisole diluted in M9 buffer. Images were acquired with an Andor iXon-888 EMCCD camera
594 (Oxford Instruments, England), with an exposure time of 150 ms and an electron-multiplying (EM)
595 gain of 200. Acquisition settings were kept constant across experiments.

596

597 **Statistical Analysis –** Behavior measurements were calculated for each individual chamber, and
598 these chamber-specific values were then used to generate the final mean values shown in the bar
599 plots. The sample size was defined as the number (approximately 25) of chambers analyzed per
600 experiment. An unpaired Student's t-test with Bonferroni correction was used to compare average
601 speeds between uniform and binary chambers. To quantify the relative difference between groups,
602 we calculated the percent change for each value in the uniform chambers relative to the mean of
603 value from the binary chambers. Specifically, we subtracted the mean of the values from the binary
604 chamber from each individual value in the uniform chamber. The result was then divided by the mean
605 of the binary chamber and multiplied by 100 to express the difference as a percentage. For
606 comparisons among multiple strains, we conducted one-way ANOVA followed by a Tukey–Kramer
607 post hoc test on all possible pairwise comparisons. All statistical analyses were performed using R.

608

609 **DATA AVAILABILITY**

610 The data supporting the findings of this study are available in Dryad at
611 https://doi.org/10.5061/dryad.k3j9kd5pz.

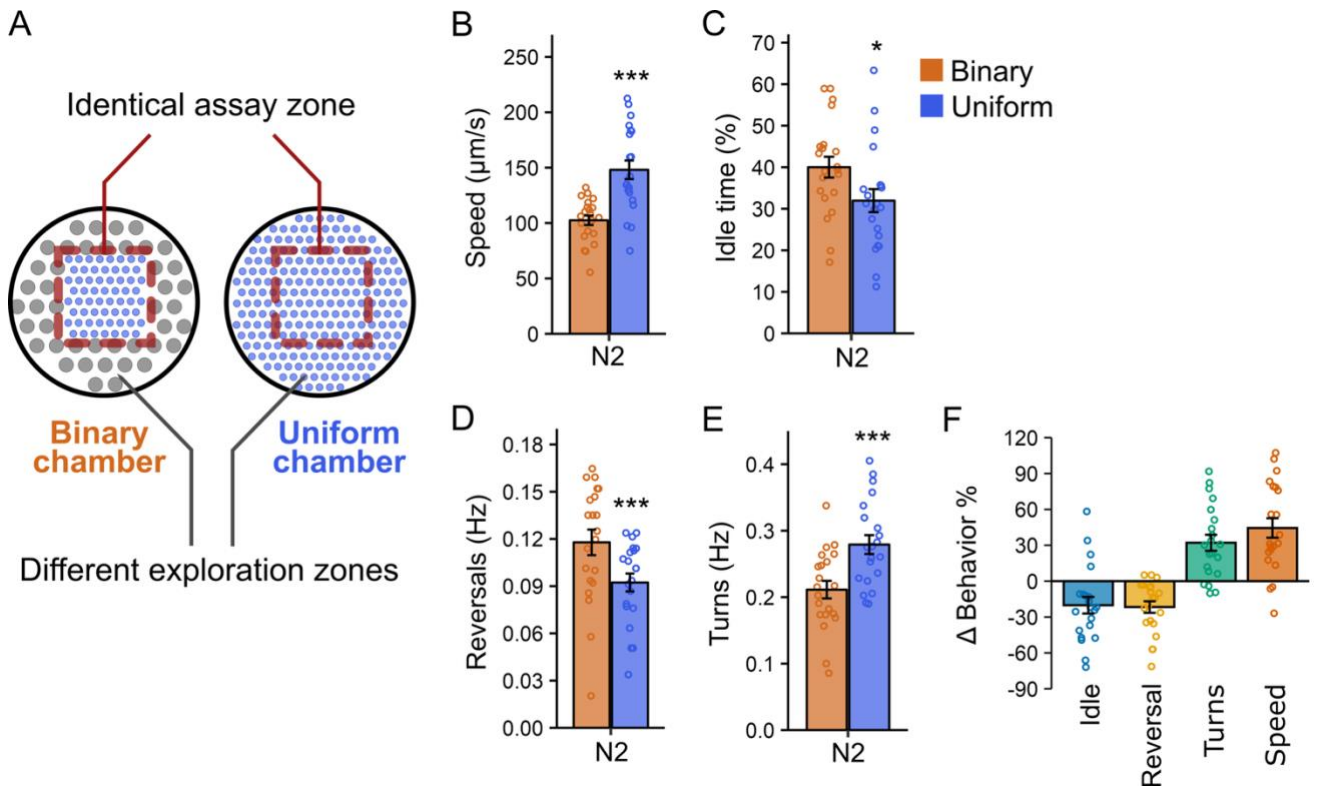

Figure 1. *C. elegans* displays distinct locomotion in identical environments after exploring different surrounding areas. (A) Schematic of two microfluidic chamber designs: uniform and binary. Both chambers contain an identical assay area (red dashed-line boxes) where locomotion was analyzed, while the surrounding exploration zones differ in PDMS pillar arrangement. (B-E) Quantification of locomotion in the assay area after 1 hour of exploration. Data from binary chambers (n = 21) are shown in orange and from uniform (n = 21) chambers in blue. Shown are (B) locomotion speed, (C) percentage of time spent idle, (D) reversal frequency, and (E) turning frequency. Statistical significance was determined using an unpaired Student's t-test (***$p < 0.001$, *$p < 0.05$). Mean ± SEM; each point represents the mean behavioral value of all worms within one chamber. (F) Percent change in each locomotion metric (speed, idle time, reversal frequency, and turning frequency), calculated from panels B-E and normalized to the mean value in binary chambers. Mean ± SEM; each point represents the mean behavioral value of all worms within one chamber.

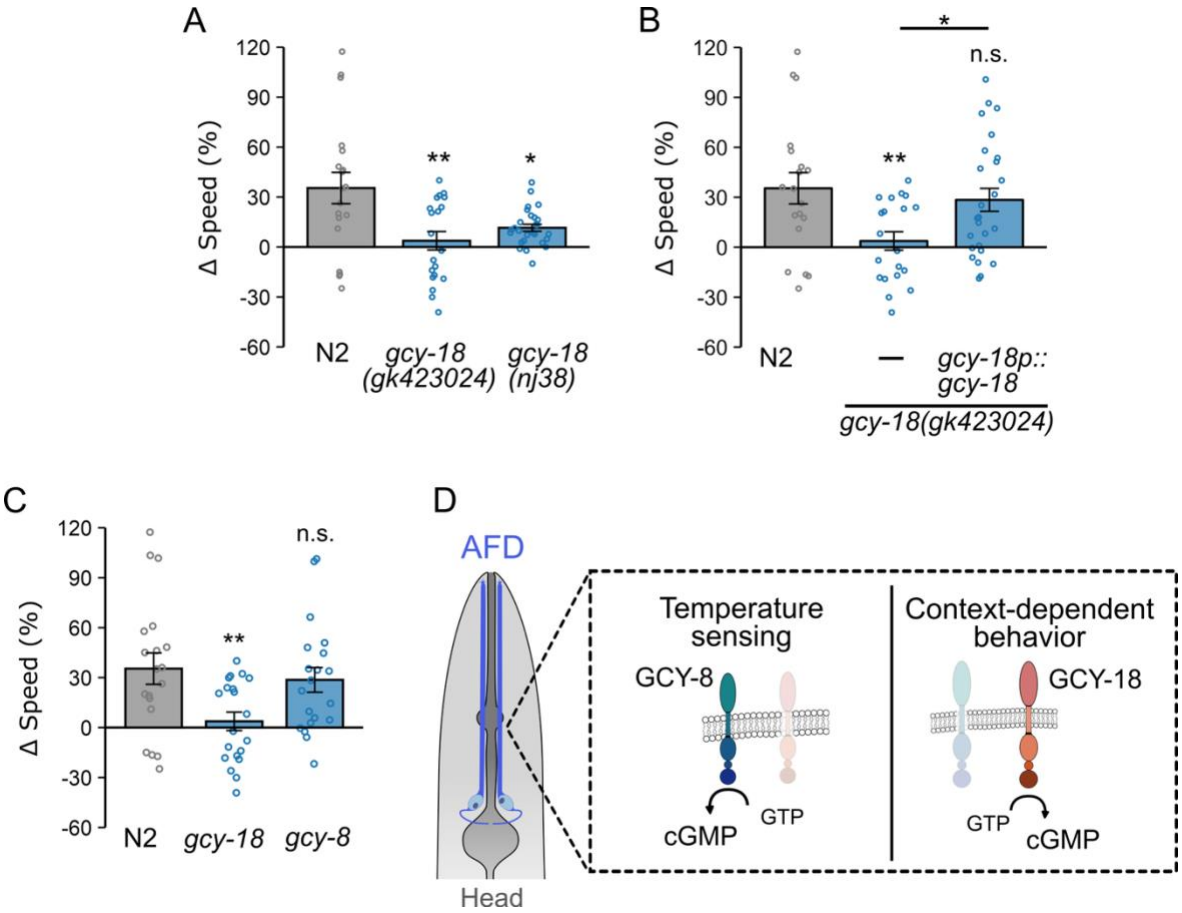

Figure 2. Guanylate cyclase gene *gcy-18* functions in AFD to mediate context-dependent locomotion modulation. (A) Difference in locomotion speed (Δspeed) between uniform and binary chambers of wild type N2 (uniform: n = 19; binary: n = 20), *gcy-18(gk423024)* mutant (uniform: *n* = 20; binary: n = 28), and *gcy-18(nj38) mutant* (uniform: *n* = 27, binary: n = 27) . ΔSpeed was calculated as the percent change in locomotion speed in uniform chambers, relative to the mean speed measured in binary chambers (see Methods). Mutant worms lacking *gcy-18* failed to demonstrate context-dependent locomotion adjustments in locomotion speed, as indicated by a low Δspeed value. (B) Δspeed of wild type, *gcy-18* mutants, and *gcy-18* mutant worms carrying a single-copy transgene expressing *gcy-18* under the control of the *gcy-18* promoter. Expression of *gcy-18p::gcy-18* restored Δspeed (uniform: n= 26; binary: n = 24). (C) Locomotion speed adjustment of N2, *gcy-18* mutants, and *gcy-8* mutant worms (uniform: n = 20, binary: n = 18). Disruption of *gcy-8* does not impair context-dependent locomotion modulation. (D) Schematic illustrating the distinct roles of guanylate cyclase genes in AFD sensory neurons: *gcy-8* is required for thermosensation but not for context-dependent locomotion

639 modulation, whereas *gcy-18* is essential for context-dependent locomotion modulation and plays only
640 a modest role in thermosensation. Data are presented as mean ± SEM. Each data point represents
641 the mean behavior of worms within a single chamber. Asterisks above bars indicate statistical
642 significance compared to wild type, whereas asterisks above horizontal black lines indicate statistical
643 significance between mutant strains. Statistical significance was determined using one-way ANOVA
644 followed by a Tukey-Kramer post hoc test (n.s.: $p > 0.05$; *: $p < 0.05$; **: $p < 0.01$).

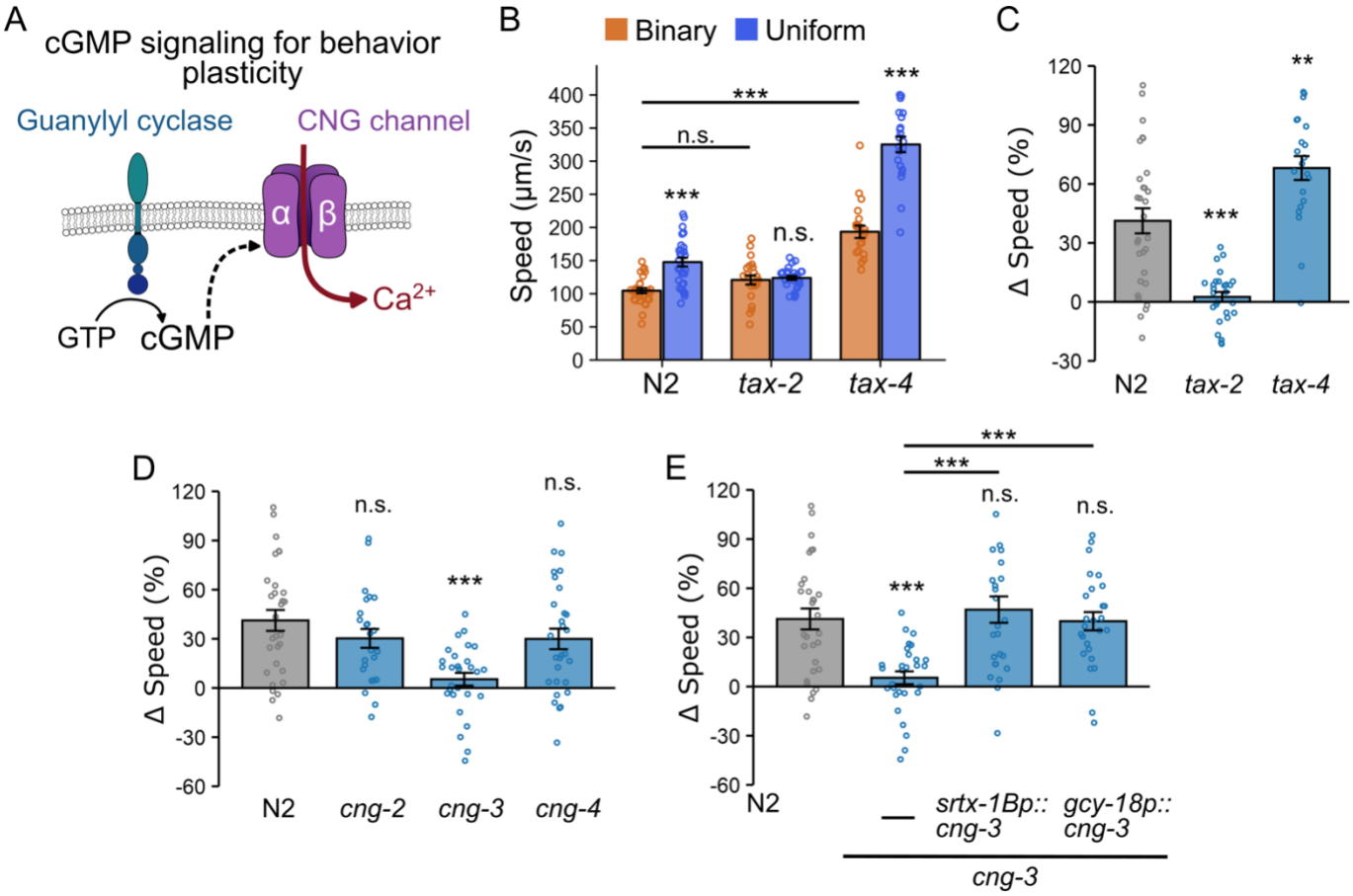

Figure 3. Cyclic nucleotide-gated (CNG) channel subunits TAX-2 and CNG-3 are required for locomotion modulation, but TAX-4 is not. (A) Schematic representation of CNG channel function. CNG channels are activated by cyclic nucleotides (such as cGMP) and mediate Ca^{2+} influx, thereby influencing neuronal activity and animal behavior. (B) Locomotion speed (μm/s) of N2 (uniform: n = 30; binary: n = 29), *tax-2* (uniform: n = 27; binary: n = 22), and *tax-4* (uniform: n = 21; binary: n = 21) mutant worms in binary (orange) and uniform (blue) chambers. The *tax-2* mutants exhibit identical locomotion rates in both chamber types, whereas worms lacking *tax-4* display accelerated basal locomotion while still preserving context-dependent locomotion modulation. Asterisks above blue bars indicate statistically significant differences in locomotion speed between uniform and binary chambers (unpaired Student's *t*-test). Asterisks above horizontal black lines indicate statistically significant differences in basal speed, defined as speed of worms in the binary chamber, between N2 and *tax-4* mutants (one-way ANOVA followed by a Tukey-Kramer post hoc test; *n.s.*: $p > 0.05$; ***: $p < 0.001$). (C) Speed differences (Δspeed) for N2, *tax-2* mutant, and *tax-4* mutant worms. The *tax-2* mutants

659 failed to modulate locomotion rates in a context-dependent manner, whereas *tax-4* mutations
660 enhanced modulation. (D) Assessment of *cng-2* (uniform: n = 24; binary: n = 22), *cng-3* (uniform: n =
661 29; binary: n = 28), and *cng-4* (uniform: n = 24; binary: n = 29) roles in locomotion adjustments. The
662 *cng-3* mutation abolishes locomotion modulation. (E) Single-copy transgenes expressing *cng-3* cDNA
663 under two AFD-specific promoters, *srtx-1bp* (uniform: n = 26; binary: n = 22) and *gcy-18p* (uniform: n =
664 26; binary: n = 25), restore context-dependent locomotion adjustments. Data are presented as mean
665 ± SEM. Each data point represents the mean behavior of worms within a single chamber. Asterisks
666 denote statistical significance versus wild type (above bars) or between mutant strains (above
667 horizontal black lines). ∆speed comparisons across strains (panels C-E) were determined using one-
668 way ANOVA followed by Tukey-Kramer post hoc tests (*: $p < 0.05$; **: $p < 0.01$, and ***: $p < 0.001$).

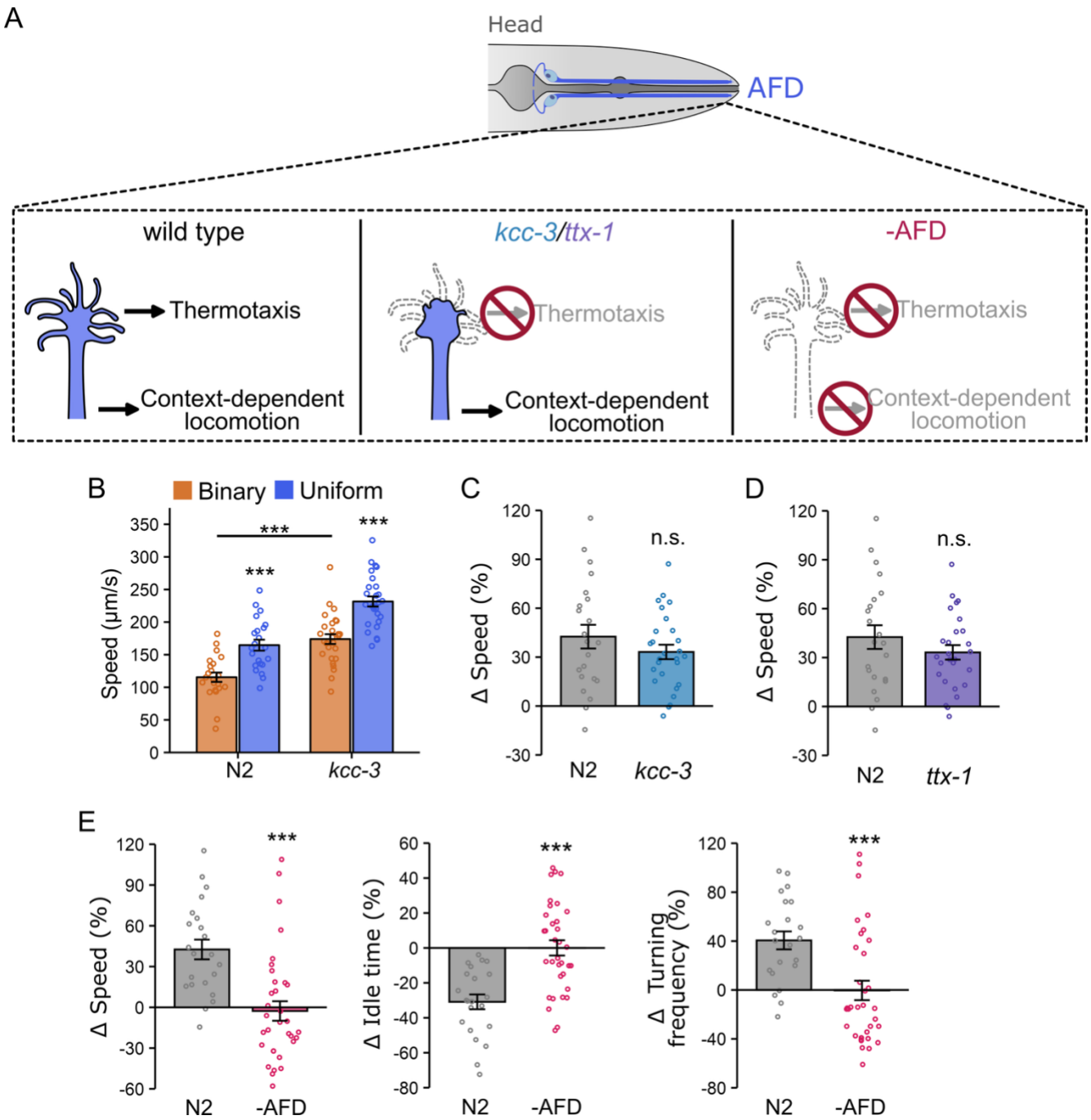

Figure 4. AFD, but not its sensory endings, is required for context-dependent locomotion modulation. (A) Schematic representation of AFD function in temperature sensing and locomotion modulation. AFD sensory endings are essential for thermosensation but dispensable for context-dependent locomotion modulation. (B) Locomotion speed (µm/s) of wild type N2 (uniform: n = 22; binary: n = 22) and *kcc-3* (uniform: n = 27; binary: n = 27) mutant worms in the binary (orange) and uniform (blue) chambers. The *kcc-3* mutants preserve context-dependent locomotion modulation while exhibiting increased basal locomotion rates. Asterisks above blue bars indicate significant differences between

677 uniform and binary chambers (unpaired Student's *t*-test). Basal speed differences in the binary
678 chambers were determined using one-way ANOVA followed by a Tukey–Kramer post hoc tests (***:
679 $p < 0.001$). (C) ∆speed of N2 and *kcc-3* mutant worms, and (D) ∆speed of N2 (uniform: n = 22; binary:
680 n = 22) and *ttx-1* (uniform: n = 27; binary: n = 27)mutant worms. Context-dependent locomotion
681 modulation remains in *kcc-3* and *ttx-1* mutant worms, although they abolish the AFD thermosensory
682 function. (E) Ablation of AFD eliminates the context-dependent modulation of speed, idle time, and
683 turning frequency (uniform: n = 34; binary: n = 36). Data are presented as mean ± SEM. Each data
684 point represents the mean behavior of worms within a single chamber. Asterisks indicate statistical
685 significance compared to wild type. ∆speed across strains (panels C-E) was analyzed by one-way
686 ANOVA followed by Tukey-Kramer post hoc tests (n.s.: $p > 0.05$, and ***: $p < 0.001$).
687

688

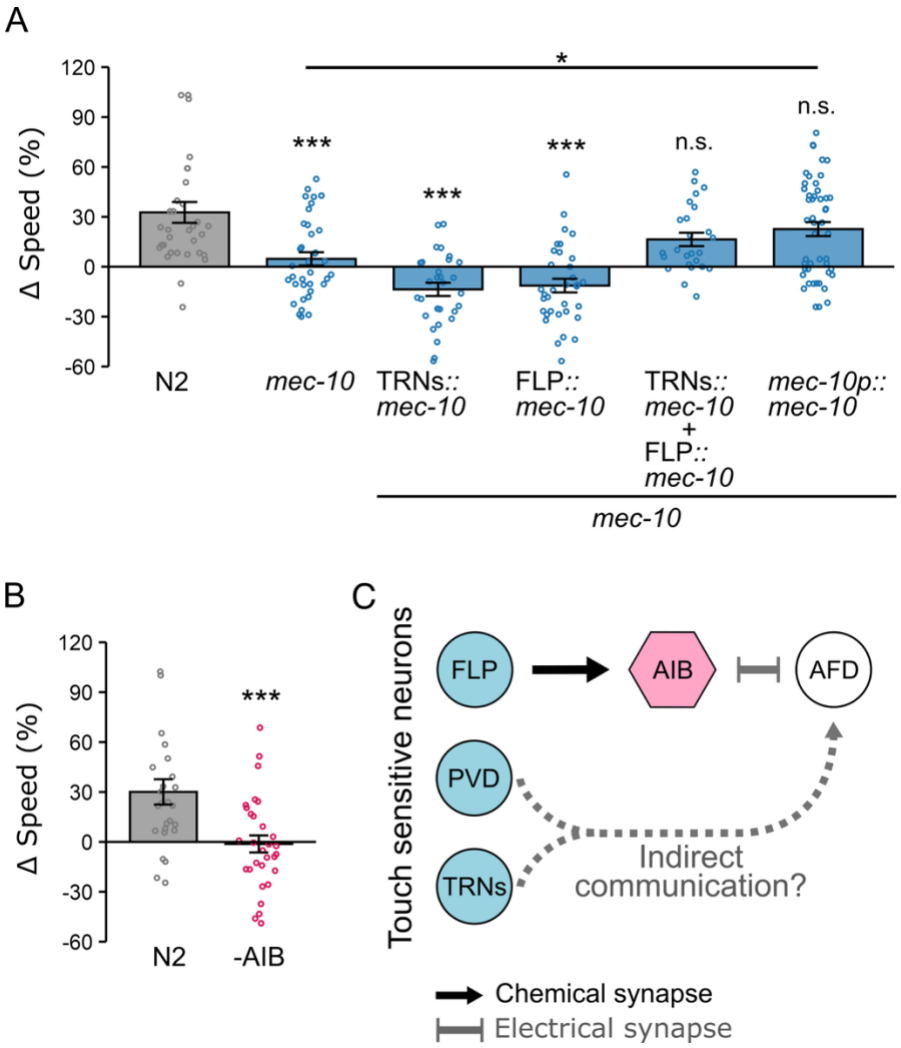

689

690 **Figure 5.** Context-dependent locomotion adjustments require the mechanosensory channel subunit
691 MEC-10 and the interneuron AIB. (A) Δspeed of wild type (uniform: n = 26; binary n = 22), *mec-10*
692 mutants (uniform: n = 30; binary n = 21), and *mec-10* mutants expressing *mec-10* cDNA under cell-
693 specific promoters: *mec-18p* (TRNs; uniform: n = 29; binary n = 25), *egl-44p* (FLP; uniform: n = 27;
694 binary n = 34), or *mec-10p* (TRNs, FLP, and PVD; uniform: n = 32; binary n = 26). (B) Δspeed of wild
695 type and AIB-ablated worms (uniform: n = 30; binary n = 30). AIB ablation abolishes speed
696 modulation. Data are shown as mean ± SEM; each data point represents the average speed of
697 worms in a single chamber. Asterisks indicate statistical significance compared to wild type (one-way
698 ANOVA followed by Tukey-Kramer post hoc tests; ***$p < 0.001$). (C) Schematic illustrating a circuit

699 framework connecting *mec-10* expressing neurons, AIB, and AFD in tactile-dependent modulation of

700 locomotion.

701

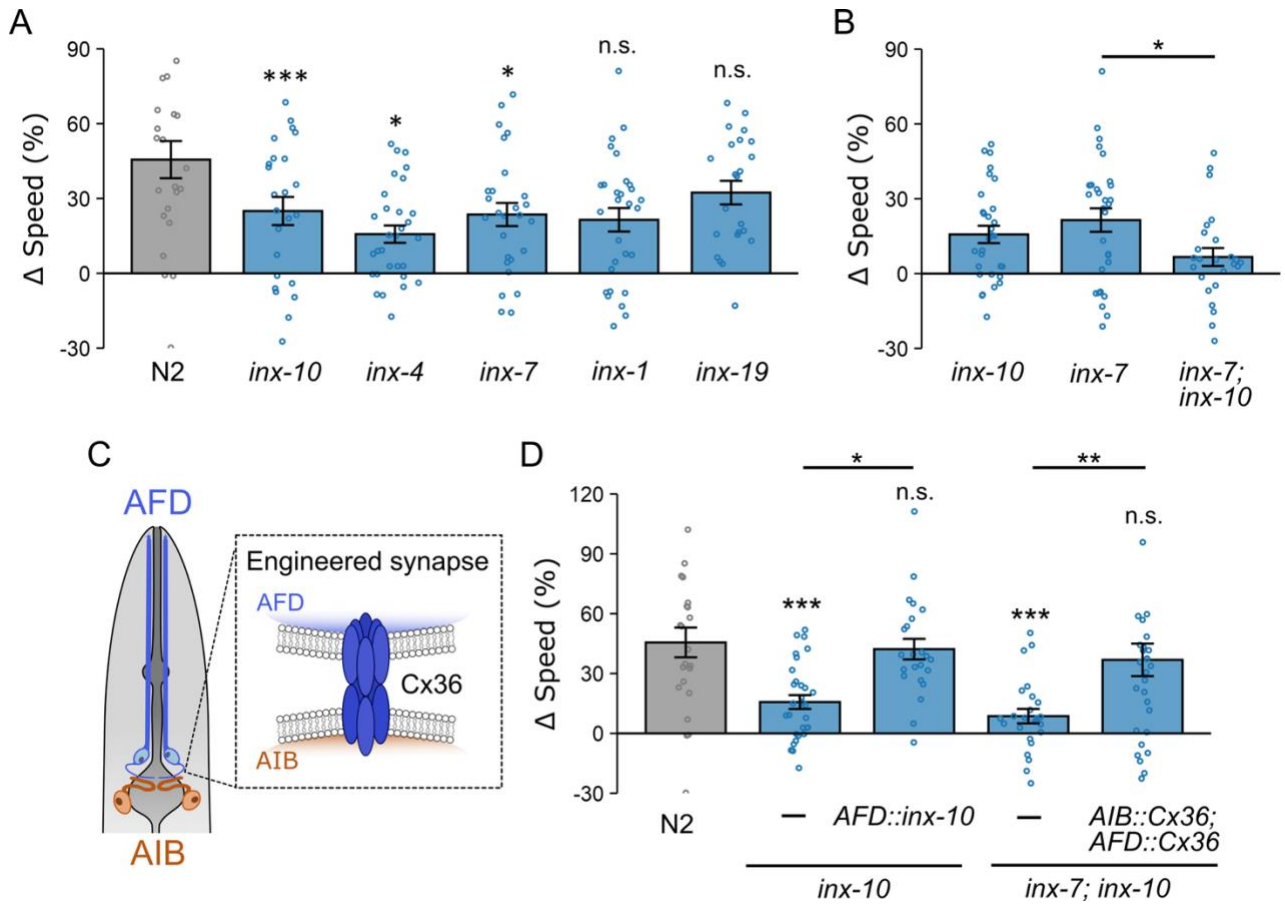

Figure 6. Tactile-dependent locomotion modulation is disrupted in mutant worms lacking gap junction genes and is restored by engineered Cx36 electrical synapses linking AFD and AIB. (A) Speed differences (Δspeed) for wild type worms (uniform: n = 23; binary: n = 25) and *inx-1* (uniform: n = 24, ; binary: n = 24), *inx-4* (uniform: n = 27; binary: n = 26), *inx-7* (uniform: n = 29; binary: n= 30), *inx-10* (uniform: n = 30; binary: n = 29), *inx-19* (uniform: n = 23; binary: n = 24) mutants. (B) Speed differences for *inx-7; inx-10* double mutants (uniform: n = 25; binary: n = 27). (C) Schematic illustrating engineered electrical synapses formed by Cx36 when expressed in adjacent neurons. (D) AFD-specific expression of *inx-10* cDNA restored tactile-dependent locomotion modulation in *inx-10* mutant worms (*srtx-1bp*; uniform: n = 23; binary: n = 24). Expression of Cx36 in both AFD (*srtx-1bp*) and AIB (*inx-1p*) similarly restored modulation in *inx-7; inx-10* double mutants (uniform: n = 30; binary: n = 28). Data are presented as mean ± SEM. Asterisks denote statistical significance versus wild type (above bars) or between indicated genotypes (above horizontal black lines). Each data point represents the mean behavior of worms within a single chamber. Statistical significance was

716 determined using one-way ANOVA followed by Tukey-Kramer post hoc tests (*: $p < 0.05$; **: $p < 0.01$,

717 and ***: $p < 0.001$).

718

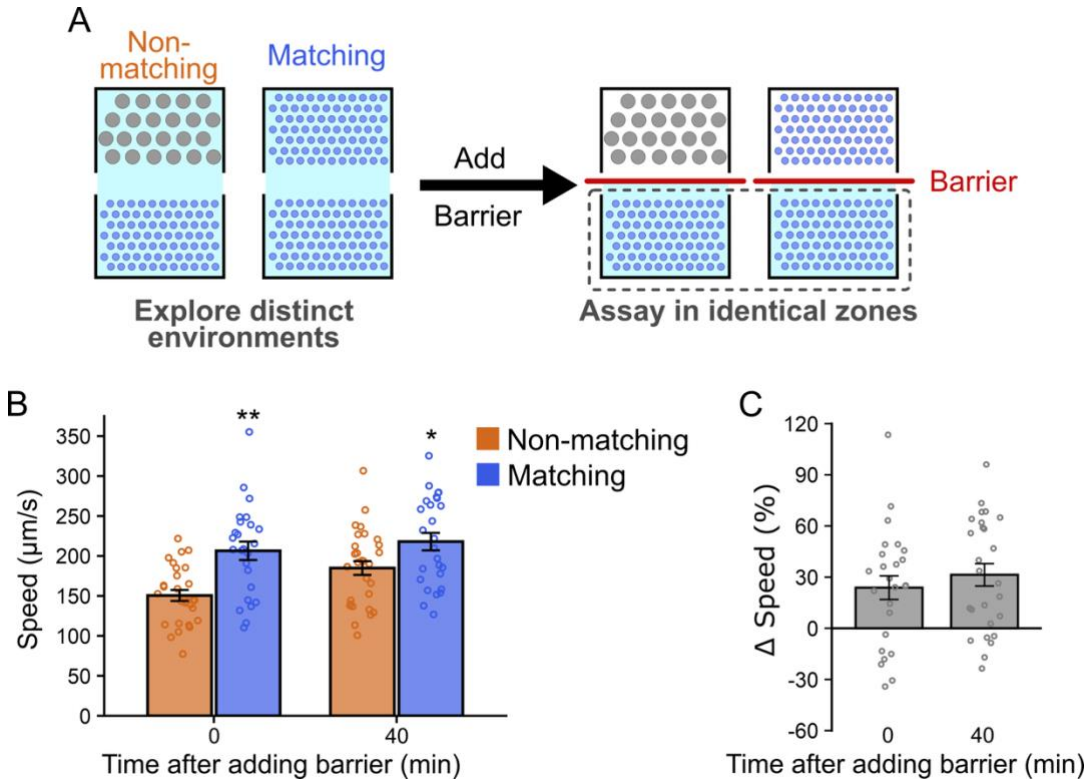

Figure 1–Supplement 1. Prior exploration of distinct physical settings modulates locomotion speed of worms in identical environments. (A) Schematic of the chamber design with separate exploration and assay zones divided by a removable barrier. The assay zone was identical across conditions, whereas the exploration zone contained physical settings that were either matching or non-matching relative to the assay zone. Worms explored these settings before entering the assay zone, where they were confined by insertion of a barrier. (B) Quantification of locomotion speed for wild type N2 worms in the assay area was performed either immediately after inserting the barrier or 40 minutes later (matching: n = 25; non-matching: n = 28). Asterisks indicate statistically significant difference between matching and non-matching chambers (unpaired Student's *t*-test; *: $p < 0.05$; **: $p < 0.01$). (C) The percent change in locomotion speed (Δspeed) between worms that had explored matching and non-matching chambers was calculated and normalized to the mean value of the non-matching condition. Data are presented as mean ± SEM, with each point representing the mean value of worms within a single chamber.

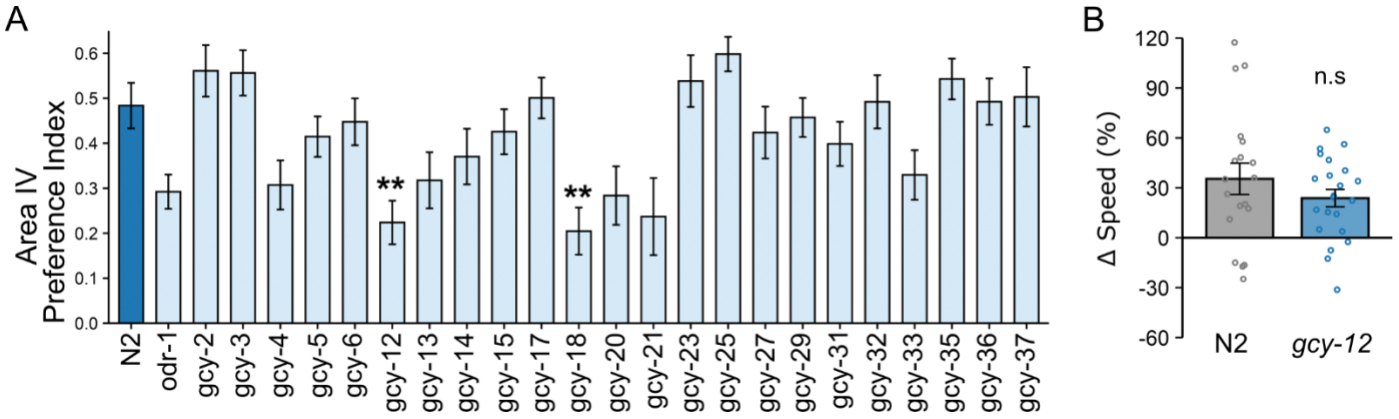

Figure 2–Supplement 1. Guanylyl cyclase genes *gcy-18* and *gcy-12* are required for spatial preference, but only *gcy-18* supports context-dependent locomotion modulation. (A) A small-scale screen of guanylyl cyclase genes required for spatial preference in microfluidic chambers. Preference index values were calculated as previously described [52]. Wild type worms exhibited a strong preference for area IV, the preferred region of the chamber [52], whereas *gcy-18(gk423024)* and *gcy-12(gk142661)* mutants showed significantly reduced preference. Data are shown as mean ± SEM; each point represents the mean value from one chamber. Statistical comparisons were performed using Dunnett's test for multiple comparisons (** $p < 0.01$). (B) Speed differences (Δspeed) between uniform and binary chambers in wild type N2 and *gcy-12* mutant worms. *gcy-12* mutants displayed context-dependent locomotion modulation comparable to wild type. Data are shown as mean ± SEM; each point represents the mean behavior of worms within a single chamber. Statistical significance was determined using an unpaired Student's t-test (n.s., $p > 0.05$).

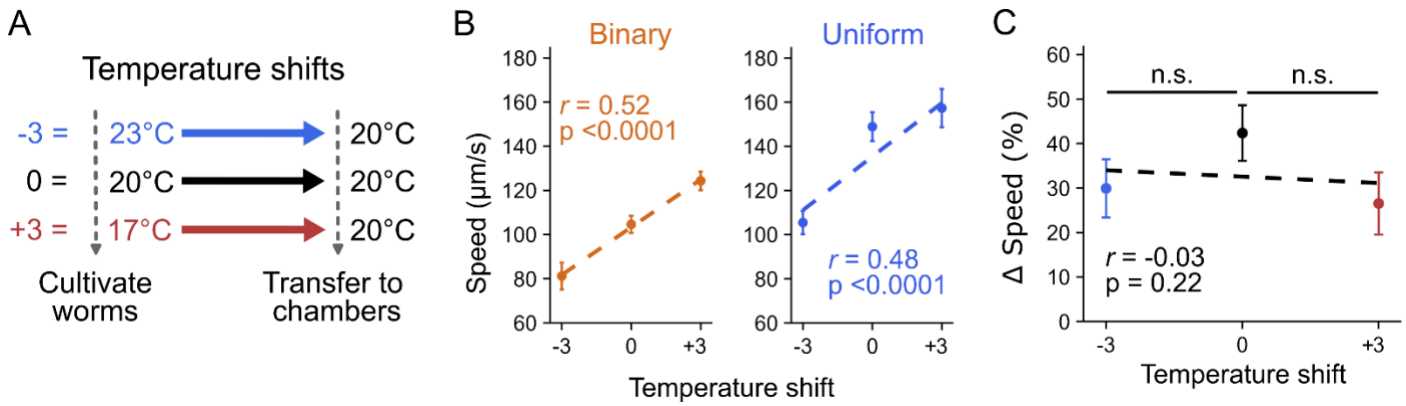

Figure 3–Supplement 1. Temperature shifts alter absolute locomotion speed but do not affect context-dependent locomotion modulation. (A) Experimental design. Worms were cultivated at 17°C, 20°C, or 23°C and then transferred to 20°C for 1 hour before behavioral recording. (B) Locomotion speed of wild type N2 worms in the binary (left) and uniform (right) chambers after experiencing temperature shifts (+3°C: uniform n = 32; binary n = 31; 0°C: uniform n = 30; binary n = 29; -3°C: uniform n = 36; binary n = 35). Linear regression identified a significant positive correlation between rearing temperature and locomotion speed in both chambers. (C) Differences in speed (Δspeed) across temperature-shift conditions. Linear regression analysis revealed no significant relationship between Δspeed and temperature shift. Data are shown as mean ± SEM.

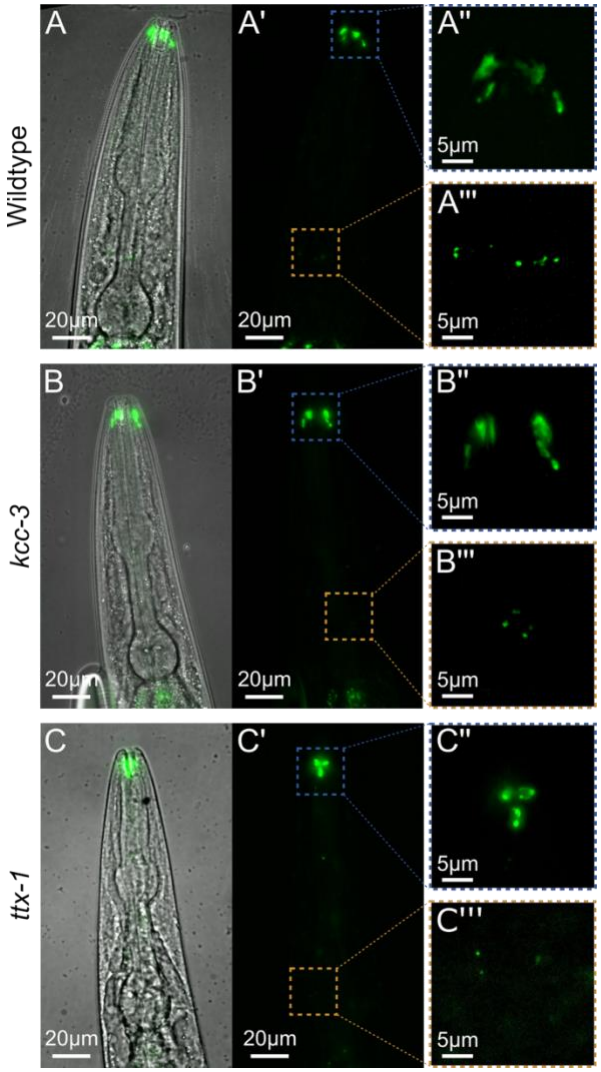

Fig. 4–Supplement 1. GCY-18 primarily localizes to AFD dendritic endings and remains detectable in *kcc-3* and *ttx-1* mutants. GCY-18 was visualized using a split-GFP strategy (GCY-18::GFP11x7 complemented by GFP1-10). (A-C) Representative images of the head region of wild type (A), *kcc-3* mutant (B), and *ttx-1* mutant (C) worms. Left panels show brightfield images overlaid with GFP fluorescence. Middle panels (A′-C′) show GFP fluorescence alone. Right panels show higher-magnification views of the distal dendritic ending (nose region; A’’-C’’) and regions near the AFD soma and axon (A’’’-C’’’). Dashed boxes in the middle panels indicate the approximate regions shown at higher magnification in the right panels.

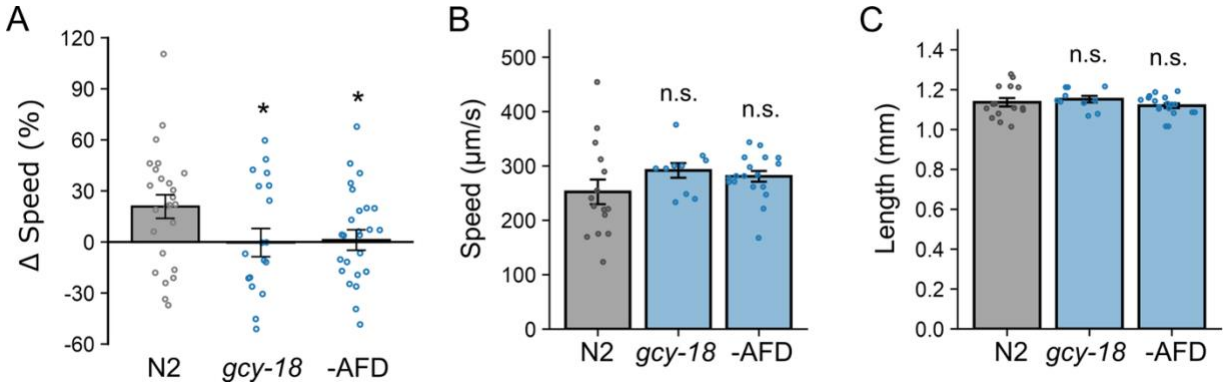

Figure 4–Supplement 2. (A) AFD-ablated and *gcy-18* mutant worms that experienced different exploration zones show impaired locomotion speed adjustment when confined to the assay zone by a removable barrier. ∆speed values for wild type N2 (matching: n = 25; non-matching: n = 28), *gcy-18* mutants (matching: n = 22; non-matching: n = 17), and AFD-ablated worms (matching: n = 26; non-matching: n = 26). Data are presented as mean ± SEM, with each point representing the mean locomotion speed value of worms within a single chamber. (B) Locomotion rates of wild type (n = 15), *gcy-18* mutants (n = 10), and AFD-ablated worms (n = 18) are comparable on NGM plates. (C) Body lengths of wild type, *gcy-18* mutant, and AFD-ablated worms are not significantly different. Data are shown as Mean ± SEM, with each point representing an individual animal (Dunnett's test, *$p < 0.05$; n.s., $p > 0.05$).

778 **S1. Table: Strains used in this study**

Strain	Genotype	Source
CX2065	*odr-1(n1936) X*	CGC
VC3024	*gcy-2(ok3721) II*	CGC
VC2796	*gcy-3(gk1154) II*	CGC
VC20038	*gcy-4(gk152604) II*	CGC
VC20321	*gcy-6(gk245152) V*	CGC
RB1000	*gcy-5(ok921) II*	CGC
VC20321	*gcy-6(gk245152) V*	CGC
VC20451	*gcy-12(gk142661) II*	CGC
VC3242	*gcy-13(gk3189) V*	CGC
JN1194	*gcy-14(pe1102) V*	CGC
VC2675	*gcy-15(gk1102) II*	CGC
VC2450	*gcy-17(gk1155) I*	CGC
VC30137	*gcy-18(gk423024) IV*	CGC
RB1935	*gcy-20(ok2538) V*	CGC
VC40920	*gcy-21(gk882422) II*	CGC
RB924	*gcy-23(ok797) IV*	CGC
VC2375	*gcy-25(gk1187) IV*	CGC
RB2622	*gcy-27(ok3653) IV*	CGC
VC20193	*gcy-29(gk162111) II*	CGC
CZ3714	*gcy-31(ok296) X*	CGC
RB1048	*gcy-32(ok995) V*	CGC
CZ3715	*gcy-33(ok232) V*	CGC
CX6448	*gcy-35(ok769) I*	CGC
AX1297	*gcy-36(db66) X*	CGC
RB626	*gcy-37(ok384) IV*	CGC
PR694	*tax-2(p694) I*	CGC
PR678	*tax-4(p678) III*	CGC
FX31482	*cng-2(tm4267) IV*	NBRP, Japan
VC40261	*cng-3(gk541751) IV*	CGC
VC20290	*cng-4(gk195496) IV*	CGC
IK800	*gcy-8(oy44) IV*	CGC
IK429	*gcy-18(nj38) IV*	CGC
VC20451	*gcy-12(gk142661) II*	CGC
BJH2598	*cng-3(gk541751) IV; ttTi5605 II*	This study
BJH2596	*gcy-18(gk423024)* IV*; ttTi5605* II	This study
BJH3481	*pekSi609[gcy-18p::gcy-18::sl2::mNeonGreen::rab-3 3'utr; vha-6p::mScarlet; hygR(+)] ttTi5605 II; gcy-18(gk423024) IV*	This study
BJH3527	*pekSi655[srtx-1Bp::cng-3::sl2::mNeonGreen::rab-3 3'utr; vha-6p::mScarlet; hygR(+)] ttTi5605 II; cng-3(gk541751) IV*	This study

BJH3539	*pekSi667[gcy-18p::cng-3::sl2::mNeonGreen::unc-54 3'utr; vha-6p::mScarlet; hygR(+)] ttTi5605 II; cng-3(gk541751) IV*	This study
GN112	*pgIs2[gcy-8p::TU#813; gcy-8p::TU#814; unc-122p::gfp; gcy-8p::mCherry; gcy-8p::gfp; ttx-3p::gfp]*	CGC
LX1024	*kcc-3(ok228) II*	Gift from the Singhvi Lab
PR767	*ttx-1(p767) V*	CGC
JN578	*peIs578 [npr-9p::casp1; npr-9p::Venus; unc-122p::mCherry]*	CGC
ZB2551	*mec-10 (tm1552) X*	CGC
BJH976	*pekSi102[egl-44p::mec-10::unc-54 3'utr; neoR(+)] ttTi5605 II; mec-10(tm1552) X.*	This study
BJH977	*pekSi103[mec-18p::mec-10::unc-54 3'utr; neoR(+)] ttTi5605 II; mec-10(tm1552) X.*	This study
BJH978	*pekSi104[mec-10p::mec-10::unc-54 3'utr; neoR(+)] ttTi5605 II; mec-10(tm1552) X.*	This study
BJH4059	*pekSi102[egl-44p::mec-10::unc-54 3'utr; neoR(+)] ttTi5605 II; pekSi715[mec-18p::mec-10::unc-54 3'utr; neoR(+)] cxTi10816 IV; mec-10(tm1552) X*	This study
FG927	*inx-1(tm6662)* X.	CGC
FG0614	*inx-4 (ok2373) V*	Gift from the Ferkey lab
RB1792	*inx-7(ok2319)* IV	CGC
RB2051	*inx-10(ok2714) V*	CGC
FX01896	*inx-19 (tm1896) I*	NBRP, Japan
BJH2919	*inx-7(ok2319) IV; inx-10(ok2714) V*	This study
BJH1162	*pekEx302 [srtx-1Bp::cx36::sl2::mNeonGreen; inx-1p::cx36::sl2::mKate; Cbr-unc-119(+); unc-122p::gfp; neoR(+)]; unc-119(ed3) III; inx-7(ok2319) IV; inx-10(ok2714) V*	This study
BJH4060	*pekSi717[srtx-1Bp::inx-10a(genomic)::sl2::gfp::let-858 3' UTR; vha-6p::mScarlet; HygR(+)] ttTi5605 II; inx-10(ok2714) V*	This study
BJH833	*muIs253[eft-3p::gfp1-10::unc-54 3'utr; Cbr-unc-119(+)]; unc-119(ed3) III; gcy-18(pek331[gcy-18::gfp11x7]) IV*	This study
BJH4056	*muIs253[eft-3p::gfp1-10::unc-54 3'utr, Cbr-unc-119(+)]; kcc-3(ok228) II; gcy-18(pek331[gcy-18::gfp11x7]) IV*	This study
BJH4057	*muIs253[eft-3p::gfp1-10::unc-54 3'utr, Cbr-unc-119(+)]; gcy-18(pek331[gcy-18::gfp11x7]) IV; ttx-1(p767) V*	This study

CGC: Caenorhabditis Genetics Center.

NBRP: National BioResource Project.

S2. Table: Plasmids used to generate transgenic strains in this study

Name	Constructs

BJP-MR16	*gcy-18p::gcy-18::sl2::mNeonGreen::rab-3 3'utr; vha-6p::mScarlet::tbb-2 3'utr; hygR(+)*
BJP-MR65	*srtx-1Bp::cng-3::sl2::mNeonGreen::rab-3 3'utr; vha-6p::mScarlet::tbb-2 3'utr; hygR(+)*
BJP-MR93	*gcy-18p::cng-3::sl2::mNeonGreen::rab-3 3'utr; vha-6p::mScarlet::tbb-2 3'utr; hygR(+)*
BJP-MR96	*inx-1p::cx36::sl2::mKate::rab-3 3'utr*
BJP-MR97	*srtx-1bp::cx36::sl2::mKate::rab-3 3'utr*
BJP-A433	*mec-18p::mec-10::unc-54 3'utr; neoR(+)*
BJP-A433	*egl-44p::mec-10::unc-54 3'utr; neoR(+)*

783

REFERENCES

1. Navarro-Sánchez M, Gil-Miravet I, Montero-Caballero D, Castillo-Gómez E, Gundlach AL, Olucha-Bordonau FE. Some key parameters in contextual fear conditioning and extinction in adult rats. Behavioural Brain Research. 2024;462: 114874. doi:10.1016/j.bbr.2024.114874

2. Maren S, Phan KL, Liberzon I. The contextual brain: implications for fear conditioning, extinction and psychopathology. Nat Rev Neurosci. 2013;14: 417–428. doi:10.1038/nrn3492

3. Battaglia S, Garofalo S, di Pellegrino G. Context-dependent extinction of threat memories: influences of healthy aging. Scientific Reports. 2018;8: 12592. doi:10.1038/s41598-018-31000-9

4. Leitman DI, Wolf DH, Loughead J, Valdez JN, Kohler CG, Brensinger C, et al. Ventrolateral prefrontal cortex and the effects of task demand context on facial affect appraisal in schizophrenia. Soc Cogn Affect Neurosci. 2011;6: 66–73. doi:10.1093/scan/nsq018

5. Hadjikhani N, Joseph RM, Manoach DS, Naik P, Snyder J, Dominick K, et al. Body expressions of emotion do not trigger fear contagion in autism spectrum disorder. Social Cognitive and Affective Neuroscience. 2009;4: 70–78. doi:10.1093/scan/nsn038

6. Kipps CM, Nestor PJ, Acosta-Cabronero J, Arnold R, Hodges JR. Understanding social dysfunction in the behavioural variant of frontotemporal dementia: the role of emotion and sarcasm processing. Brain. 2009;132: 592–603. doi:10.1093/brain/awn314

7. Greimel E, Nehrkorn B, Fink GR, Kukolja J, Kohls G, Müller K, et al. Neural mechanisms of encoding social and non-social context information in autism spectrum disorder. Neuropsychologia. 2012;50: 3440–3449. doi:10.1016/j.neuropsychologia.2012.09.029

8. Badel L, Ohta K, Tsuchimoto Y, Kazama H. Decoding of Context-Dependent Olfactory Behavior in Drosophila. Neuron. 2016;91: 155–167. doi:10.1016/j.neuron.2016.05.022

9. Haberkern H, Basnak MA, Ahanonu B, Schauder D, Cohen JD, Bolstad M, et al. Visually Guided Behavior and Optogenetically Induced Learning in Head-Fixed Flies Exploring a Virtual Landscape. Current Biology. 2019;29: 1647-1659.e8. doi:10.1016/j.cub.2019.04.033

10. Sheintuch L, Geva N, Baumer H, Rechavi Y, Rubin A, Ziv Y. Multiple Maps of the Same Spatial Context Can Stably Coexist in the Mouse Hippocampus. Current Biology. 2020;30: 1467-1476.e6. doi:10.1016/j.cub.2020.02.018

11. Zars M, Zars T. High and low temperatures have unequal reinforcing properties in Drosophila spatial learning. J Comp Physiol A. 2006;192: 727–735. doi:10.1007/s00359-006-0109-6

12. Kishimoto Y, Kasamatsu S, Yanai S, Endo S, Akaike T, Ihara H. 8-Nitro-cGMP attenuates context-dependent fear memory in mice. Biochemical and Biophysical Research Communications. 2019;511: 141–147. doi:10.1016/j.bbrc.2019.01.138

13. Sasaki A, Sotnikova TD, Gainetdinov RR, Jarvis ED. Social Context-Dependent Singing-Regulated Dopamine. J Neurosci. 2006;26: 9010–9014. doi:10.1523/JNEUROSCI.1335-06.2006

14. Billeter J-C, Jagadeesh S, Stepek N, Azanchi R, Levine JD. Drosophila melanogaster females change mating behaviour and offspring production based on social context. Proceedings of the Royal Society B: Biological Sciences. 2012;279: 2417–2425. doi:10.1098/rspb.2011.2676

15. Wolfin MS, Raguso RA, Davidowitz G, Goyret J. Context dependency of in-flight responses by Manduca sexta moths to ambient differences in relative humidity. Journal of Experimental Biology. 2018;221. doi:10.1242/jeb.177774

16. Sawin ER, Ranganathan R, Horvitz HR. C. elegans Locomotory Rate Is Modulated by the Environment through a Dopaminergic Pathway and by Experience through a Serotonergic Pathway. Neuron. 2000;26: 619–631. doi:10.1016/S0896-6273(00)81199-X

17. Gourgou E, Adiga K, Goettemoeller A, Chen C, Hsu A-L. *Caenorhabditis elegans* learning in a structured maze is a multisensory behavior. iScience. 2021;24: 102284. doi:10.1016/j.isci.2021.102284

18. Dillon J, Holden-Dye L, O'Connor V, Hopper NA. Context-dependent regulation of feeding behaviour by the insulin receptor, DAF-2, in Caenorhabditis elegans. Invert Neurosci. 2016;16: 4. doi:10.1007/s10158-016-0187-2

19. Law E, Nuttley WM, Kooy D van der. Contextual Taste Cues Modulate Olfactory Learning in C. elegans by an Occasion-Setting Mechanism. Current Biology. 2004;14: 1303–1308. doi:10.1016/j.cub.2004.06.066

20. Kindt KS, Quast KB, Giles AC, De S, Hendrey D, Nicastro I, et al. Dopamine Mediates Context-Dependent Modulation of Sensory Plasticity in C. elegans. Neuron. 2007;55: 662–676. doi:10.1016/j.neuron.2007.07.023

21. Goetting DL, Soto R, Van Buskirk C. Food-Dependent Plasticity in Caenorhabditis elegans Stress-Induced Sleep Is Mediated by TOR-FOXA and TGF-β Signaling. Genetics. 2018;209: 1183–1195. doi:10.1534/genetics.118.301204

22. Susoy V, Hung W, Witvliet D, Whitener JE, Wu M, Park CF, et al. Natural sensory context drives diverse brain-wide activity during C. elegans mating. Cell. 2021; S0092867421009983. doi:10.1016/j.cell.2021.08.024

23. Ghosh DD, Sanders T, Hong S, McCurdy LY, Chase DL, Cohen N, et al. Neural Architecture of Hunger-Dependent Multisensory Decision Making in *C. elegans*. Neuron. 2016;92: 1049–1062. doi:10.1016/j.neuron.2016.10.030

24. Zhen M, Samuel AD. C. elegans locomotion: small circuits, complex functions. Current Opinion in Neurobiology. 2015;33: 117–126. doi:10.1016/j.conb.2015.03.009

25. Emmons SW. Neural Circuits of Sexual Behavior in Caenorhabditis elegans. Annual Review of Neuroscience. 2018;41: 349–369. doi:10.1146/annurev-neuro-070815-014056

26. Meisel JD, Kim DH. Behavioral avoidance of pathogenic bacteria by Caenorhabditis elegans. Trends in Immunology. 2014;35: 465–470. doi:10.1016/j.it.2014.08.008

27. Metaxakis A, Petratou D, Tavernarakis N. Multimodal sensory processing in Caenorhabditis elegans. Open Biol. 2018;8. doi:10.1098/rsob.180049

28. Stout Jr. RF, Verkhratsky A, Parpura V. Caenorhabditis elegans glia modulate neuronal activity and behavior. Front Cell Neurosci. 2014;8. doi:10.3389/fncel.2014.00067

29. Ward S, Thomson N, White JG, Brenner S. Electron microscopical reconstruction of the anterior sensory anatomy of the nematode caenorhabditis elegans. Journal of Comparative Neurology. 1975;160: 313–337. doi:10.1002/cne.901600305

30. Ware RW, Clark D, Crossland K, Russell RL. The nerve ring of the nematode Caenorhabditis elegans: Sensory input and motor output. Journal of Comparative Neurology. 1975;162: 71–110. doi:10.1002/cne.901620106

31. Ghosh DD, Nitabach MN, Zhang Y, Harris G. Multisensory integration in C. elegans. Current Opinion in Neurobiology. 2017;43: 110–118. doi:10.1016/j.conb.2017.01.005

32. Hobert O. Behavioral plasticity in C. elegans: Paradigms, circuits, genes. Journal of Neurobiology. 2003;54: 203–223. doi:10.1002/neu.10168

33. Komuniecki R, Hapiak V, Harris G, Bamber B. Context-dependent modulation reconfigures interactive sensory-mediated microcircuits in Caenorhabditis elegans. Current Opinion in Neurobiology. 2014;29: 17–24. doi:10.1016/j.conb.2014.04.006

34. Goodman MB, Sengupta P. The extraordinary AFD thermosensor of C. elegans. Pflugers Arch - Eur J Physiol. 2018;470: 839–849. doi:10.1007/s00424-017-2089-5

35. Clark DA, Biron D, Sengupta P, Samuel ADT. The AFD Sensory Neurons Encode Multiple Functions Underlying Thermotactic Behavior in Caenorhabditis elegans. J Neurosci. 2006;26: 7444–7451. doi:10.1523/JNEUROSCI.1137-06.2006

36. Yoshida A, Nakano S, Suzuki T, Ihara K, Higashiyama T, Mori I. A glial K+/Cl− cotransporter modifies temperature-evoked dynamics in Caenorhabditis elegans sensory neurons. Genes, Brain and Behavior. 2016;15: 429–440. doi:10.1111/gbb.12260

37. Singhvi A, Liu B, Friedman CJ, Fong J, Lu Y, Huang X-Y, et al. A Glial K/Cl Transporter Controls Neuronal Receptive Ending Shape by Chloride Inhibition of an rGC. Cell. 2016;165: 936–948. doi:10.1016/j.cell.2016.03.026

38. Satterlee JS, Sasakura H, Kuhara A, Berkeley M, Mori I, Sengupta P. Specification of Thermosensory Neuron Fate in C. elegans Requires ttx-1, a Homolog of otd/Otx. Neuron. 2001;31: 943–956. doi:10.1016/S0896-6273(01)00431-7

39. Aok I, Shiota M, Tsukada Y, Nakano S, Mori I. cGMP dynamics that underlies thermosensation in temperature-sensing neuron regulates thermotaxis behavior in C. elegans. PLOS ONE. 2022;17: e0278343. doi:10.1371/journal.pone.0278343

40. Ramot D, MacInnis BL, Goodman MB. Bidirectional temperature-sensing by a single thermosensory neuron in C. elegans. Nat Neurosci. 2008;11: 908–915. doi:10.1038/nn.2157

41. Wang D, O'Halloran D, Goodman MB. GCY-8, PDE-2, and NCS-1 are critical elements of the cGMP-dependent thermotransduction cascade in the AFD neurons responsible for C. elegans thermotaxis. J Gen Physiol. 2013;142: 437–449. doi:10.1085/jgp.201310959

42. Takeishi A, Yu YV, Hapiak VM, Bell HW, O'Leary T, Sengupta P. Receptor-type Guanylyl Cyclases Confer Thermosensory Responses in C. elegans. Neuron. 2016;90: 235–244. doi:10.1016/j.neuron.2016.03.002

899 43. Inada H, Ito H, Satterlee J, Sengupta P, Matsumoto K, Mori I. Identification of Guanylyl
900 Cyclases That Function in Thermosensory Neurons of Caenorhabditis elegans. Genetics.
901 2006;172: 2239–2252. doi:10.1534/genetics.105.050013

902 44. Hedgecock EM, Russell RL. Normal and mutant thermotaxis in the nematode Caenorhabditis
903 elegans. Proc Natl Acad Sci USA. 1975;72: 4061–4065. doi:10.1073/pnas.72.10.4061

904 45. Ryu WS, Samuel ADT. Thermotaxis in *Caenorhabditis elegans* Analyzed by Measuring
905 Responses to Defined Thermal Stimuli. J Neurosci. 2002;22: 5727–5733.
906 doi:10.1523/JNEUROSCI.22-13-05727.2002

907 46. Kuhara A, Ohnishi N, Shimowada T, Mori I. Neural coding in a single sensory neuron controlling
908 opposite seeking behaviours in Caenorhabditis elegans. Nat Commun. 2011;2: 355.
909 doi:10.1038/ncomms1352

910 47. Mori I, Ohshima Y. Neural regulation of thermotaxis in Caenorhabditis elegans. Nature.
911 1995;376: 344–348. doi:10.1038/376344a0

912 48. Kuhara A, Mori I. Molecular Physiology of the Neural Circuit for Calcineurin-Dependent
913 Associative Learning in *Caenorhabditis elegans*. J Neurosci. 2006;26: 9355–9364.
914 doi:10.1523/JNEUROSCI.0517-06.2006

915 49. Hobert O, D'Alberti T, Liu Y, Ruvkun G. Control of Neural Development and Function in a
916 Thermoregulatory Network by the LIM Homeobox Gene lin-11. J Neurosci. 1998;18: 2084–
917 2096. doi:10.1523/JNEUROSCI.18-06-02084.1998

918 50. Chung SH, Clark DA, Gabel CV, Mazur E, Samuel AD. The role of the AFD neuron in C.
919 elegans thermotaxis analyzed using femtosecond laser ablation. BMC Neurosci. 2006;7: 30.
920 doi:10.1186/1471-2202-7-30

921 51. Ikeda M, Nakano S, Giles AC, Xu L, Costa WS, Gottschalk A, et al. Context-dependent
922 operation of neural circuits underlies a navigation behavior in Caenorhabditis elegans. PNAS.
923 2020;117: 6178–6188. doi:10.1073/pnas.1918528117

924 52. Han B, Dong Y, Zhang L, Liu Y, Rabinowitch I, Bai J. Dopamine signaling tunes spatial pattern
925 selectivity in C. elegans. eLife. 2017;6. doi:10.7554/eLife.22896

926 53. Komatsu H, Jin Y-H, L'Etoile N, Mori I, Bargmann CI, Akaike N, et al. Functional reconstitution of
927 a heteromeric cyclic nucleotide-gated channel of Caenorhabditis elegans in cultured cells. Brain
928 Research. 1999;821: 160–168. doi:10.1016/S0006-8993(99)01111-7

929 54. Finn JT, Krautwurst D, Schroeder JE, Chen T-Y, Reed RR, Yau K-W. Functional Co-assembly
930 among Subunits of Cyclic-Nucleotide-Activated, Nonselective Cation Channels, and Across
931 Species from Nematode to Human. Biophysical Journal. 1998;74: 1333–1345.
932 doi:10.1016/S0006-3495(98)77846-4

933 55. Kaupp UB, Seifert R. Cyclic Nucleotide-Gated Ion Channels. Physiological Reviews. 2002;82:
934 769–824. doi:10.1152/physrev.00008.2002

935 56. Xue J, Han Y, Zeng W, Jiang Y. Structural mechanisms of assembly, permeation, gating, and
936 pharmacology of native human rod CNG channel. Neuron. 2022;110: 86-95.e5.
937 doi:10.1016/j.neuron.2021.10.006

938 57. Harris G, Shen Y, Ha H, Donato A, Wallis S, Zhang X, et al. Dissecting the Signaling
939 Mechanisms Underlying Recognition and Preference of Food Odors. J Neurosci. 2014;34:
940 9389–9403. doi:10.1523/JNEUROSCI.0012-14.2014

941 58. He C, Altshuler-Keylin S, Daniel D, L'Etoile -->Noelle D., O'Halloran D. The cyclic nucleotide
942 gated channel subunit CNG-1 instructs behavioral outputs in Caenorhabditis elegans by
943 coincidence detection of nutritional status and olfactory input. Neuroscience Letters. 2016;632:
944 71–78. doi:10.1016/j.neulet.2016.08.037

945 59. Herrero A, Yoshii T, Ispizua JI, Colque C, Veenstra JA, Muraro NI, et al. Coupling Neuropeptide
946 Levels to Structural Plasticity in Drosophila Clock Neurons. Current Biology. 2020;30: 3154-
947 3166.e4. doi:10.1016/j.cub.2020.06.009

948 60. Feketa VV, Nikolaev YA, Merriman DK, Bagriantsev SN, Gracheva EO. CNGA3 acts as a cold
949 sensor in hypothalamic neurons. Lishko PV, Aldrich RW, Tominaga M, Sobolevsky A, editors.
950 eLife. 2020;9: e55370. doi:10.7554/eLife.55370

951 61. Dolzer J, Schröder K, Stengl M. Cyclic nucleotide-dependent ionic currents in olfactory receptor
952 neurons of the hawkmoth Manduca sexta suggest pull–push sensitivity modulation. European
953 Journal of Neuroscience. 2021;54: 4804–4826. doi:10.1111/ejn.15346

954 62. Kelliher KR, Ziesmann J, Munger SD, Reed RR, Zufall F. Importance of the CNGA4 channel
955 gene for odor discrimination and adaptation in behaving mice. Proceedings of the National
956 Academy of Sciences. 2003;100: 4299–4304. doi:10.1073/pnas.0736071100

957 63. Michalakis S, Kleppisch T, Polta SA, Wotjak CT, Koch S, Rammes G, et al. Altered synaptic
958 plasticity and behavioral abnormalities in CNGA3-deficient mice. Genes, Brain and Behavior.
959 2011;10: 137–148. doi:10.1111/j.1601-183X.2010.00646.x

960 64. Haverkamp S, Michalakis S, Claes E, Seeliger MW, Humphries P, Biel M, et al. Synaptic
961 Plasticity in CNGA3−/− Mice: Cone Bipolar Cells React on the Missing Cone Input and Form
962 Ectopic Synapses with Rods. J Neurosci. 2006;26: 5248–5255. doi:10.1523/JNEUROSCI.4483-
963 05.2006

964 65. Komatsu H, Mori I, Rhee J-S, Akaike N, Ohshima Y. Mutations in a Cyclic Nucleotide–Gated
965 Channel Lead to Abnormal Thermosensation and Chemosensation in C. elegans. Neuron.
966 1996;17: 707–718. doi:10.1016/S0896-6273(00)80202-0

967 66. Kimura KD, Miyawaki A, Matsumoto K, Mori I. The *C. elegans* Thermosensory Neuron AFD
968 Responds to Warming. Current Biology. 2004;14: 1291–1295. doi:10.1016/j.cub.2004.06.060

969 67. Parida L, Neogi S, Padmanabhan V. Effect of Temperature Pre-Exposure on the Locomotion
970 and Chemotaxis of C. elegans. PLOS ONE. 2014;9: e111342.
971 doi:10.1371/journal.pone.0111342

972 68. Altanbadralt M, Basutta J, Hajen K, Parmar J, Sidhu BV. The effect of temperature on the speed
973 of locomotion in *Caenorhabditis elegans*. The Expedition. 2015;5. Available:
974 https://ojs.library.ubc.ca/index.php/expedition/article/view/188343

975 69. Wojtyniak M, Brear AG, O'Halloran DM, Sengupta P. Cell- and subunit-specific mechanisms of
976 CNG channel ciliary trafficking and localization in C. elegans. J Cell Sci. 2013;126: 4381–4395.
977 doi:10.1242/jcs.127274

70. Hill TJ, Sengupta P. Feedforward and feedback mechanisms cooperatively regulate rapid experience-dependent response adaptation in a single thermosensory neuron type. bioRxiv; 2023. p. 2023.12.05.570166. doi:10.1101/2023.12.05.570166

71. Cho S-W, Choi KY, Park C-S. A new putative cyclic nucleotide-gated channel gene, cng-3, is critical for thermotolerance in Caenorhabditis elegans. Biochemical and Biophysical Research Communications. 2004;325: 525–531. doi:10.1016/j.bbrc.2004.10.060

72. Kagoshima H, Kohara Y. Co-expression of the transcription factors CEH-14 and TTX-1 regulates AFD neuron-specific genes gcy-8 and gcy-18 in C. elegans. Developmental Biology. 2015;399: 325–336. doi:10.1016/j.ydbio.2015.01.010

73. He S, Cuentas-Condori A, Miller DM III. NATF (Native and Tissue-Specific Fluorescence): A Strategy for Bright, Tissue-Specific GFP Labeling of Native Proteins in Caenorhabditis elegans. Genetics. 2019;212: 387–395. doi:10.1534/genetics.119.302063

74. Harris N, Bates SG, Zhuang Z, Bernstein M, Stonemetz JM, Hill TJ, et al. Molecular encoding of stimulus features in a single sensory neuron type enables neuronal and behavioral plasticity. Current Biology. 2023;0. doi:10.1016/j.cub.2023.02.073

75. Nguyen PAT, Liou W, Hall DH, Leroux MR. Ciliopathy proteins establish a bipartite signaling compartment in a C. elegans thermosensory neuron. Journal of Cell Science. 2014;127: 5317–5330. doi:10.1242/jcs.157610

76. Glauser DA, Chen WC, Agin R, MacInnis BL, Hellman AB, Garrity PA, et al. Heat Avoidance Is Regulated by Transient Receptor Potential (TRP) Channels and a Neuropeptide Signaling Pathway in Caenorhabditis elegans. Genetics. 2011;188: 91–103. doi:10.1534/genetics.111.127100

77. Árnadóttir J, O'Hagan R, Chen Y, Goodman MB, Chalfie M. The DEG/ENaC Protein MEC-10 Regulates the Transduction Channel Complex in Caenorhabditis elegans Touch Receptor Neurons. J Neurosci. 2011;31: 12695–12704. doi:m

78. Chatzigeorgiou M, Grundy L, Kindt KS, Lee W-H, Driscoll M, Schafer WR. Spatial Asymmetry in the Mechanosensory Phenotypes of the C. elegans DEG/ENaC Gene mec-10. Journal of Neurophysiology. 2010;104: 3334–3344. doi:10.1152/jn.00330.2010

79. Huang M, Chalfie M. Gene interactions affecting mechanosensory transduction in Caenorhabditis elegans. Nature. 1994;367: 467–470. doi:10.1038/367467a0

80. Zhang S, Ma C, Chalfie M. Combinatorial Marking of Cells and Organelles with Reconstituted Fluorescent Proteins. Cell. 2004;119: 137–144. doi:10.1016/j.cell.2004.09.012

81. Wu J, Duggan A, Chalfie M. Inhibition of touch cell fate by egl-44 and egl-46 in C. elegans. Genes Dev. 2001;15: 789–802. doi:10.1101/gad.857401

82. Kunitomo H, Sato H, Iwata R, Satoh Y, Ohno H, Yamada K, et al. Concentration memory-dependent synaptic plasticity of a taste circuit regulates salt concentration chemotaxis in Caenorhabditis elegans. Nat Commun. 2013;4: 2210. doi:10.1038/ncomms3210

83. Güiza J, Barría I, Sáez JC, Vega JL. Innexins: Expression, Regulation, and Functions. Frontiers in Physiology. 2018;9: 1414. doi:10.3389/fphys.2018.01414

017 84. Altun ZF, Chen B, Wang Z-W, Hall DH. High resolution map of Caenorhabditis elegans gap
018 junction proteins. Developmental Dynamics. 2009;238: 1936–1950. doi:10.1002/dvdy.22025

019 85. Phelan P, Starich TA. Innexins get into the gap. BioEssays. 2001;23: 388–396.
020 doi:10.1002/bies.1057

021 86. Taylor SR, Santpere G, Weinreb A, Barrett A, Reilly MB, Xu C, et al. Molecular topography of an
022 entire nervous system. Cell. 2021;184: 4329-4347.e23. doi:10.1016/j.cell.2021.06.023

023 87. Rabinowitch I, Upadhyaya B, Pant A, Galski D, Kreines L, Bai J. Circumventing neural damage
024 in a C. elegans chemosensory circuit using genetically engineered synapses. Cell Systems.
025 2021;12: 263-271.e4. doi:10.1016/j.cels.2020.12.003

026 88. Choi M-K, Liu H, Wu T, Yang W, Zhang Y. NMDAR-mediated modulation of gap junction circuit
027 regulates olfactory learning in C. elegans. Nat Commun. 2020;11: 3467. doi:10.1038/s41467-
028 020-17218-0

029 89. Rabinowitch I, Chatzigeorgiou M, Zhao B, Treinin M, Schafer WR. Rewiring neural circuits by
030 the insertion of ectopic electrical synapses in transgenic C. elegans. Nat Commun. 2014;5:
031 4442. doi:10.1038/ncomms5442

032 90. Rabinowitch I, Schafer WR. Engineering new synaptic connections in the C. elegans
033 connectome. Worm. 2015;4: e992668. doi:10.4161/21624054.2014.992668

034 91. Chang AJ, Chronis N, Karow DS, Marletta MA, Bargmann CI. A Distributed Chemosensory
035 Circuit for Oxygen Preference in C. elegans. PLOS Biology. 2006;4: e274.
036 doi:10.1371/journal.pbio.0040274

037 92. Hart AC, Sims S, Kaplan JM. Synaptic code for sensory modalities revealed by C. elegans
038 GLR-1 glutamate receptor. Nature. 1995;378: 82–85. doi:10.1038/378082a0

039 93. Kaplan JM, Horvitz HR. A dual mechanosensory and chemosensory neuron in Caenorhabditis
040 elegans. Proceedings of the National Academy of Sciences. 1993;90: 2227–2231.
041 doi:10.1073/pnas.90.6.2227

042 94. Yoshida K, Hirotsu T, Tagawa T, Oda S, Wakabayashi T, Iino Y, et al. Odour concentration-
043 dependent olfactory preference change in C. elegans. Nat Commun. 2012;3: 739.
044 doi:10.1038/ncomms1750

045 95. Biron D, Wasserman S, Thomas JH, Samuel ADT, Sengupta P. An olfactory neuron responds
046 stochastically to temperature and modulates Caenorhabditis elegans thermotactic behavior.
047 Proceedings of the National Academy of Sciences. 2008;105: 11002–11007.
048 doi:10.1073/pnas.0805004105

049 96. Kuhara A, Okumura M, Kimata T, Tanizawa Y, Takano R, Kimura KD, et al. Temperature
050 Sensing by an Olfactory Neuron in a Circuit Controlling Behavior of C. elegans. Science.
051 2008;320: 803–807. doi:10.1126/science.1148922

052 97. Kano A, Matsuyama HJ, Nakano S, Mori I. AWC thermosensory neuron interferes with
053 information processing in a compact circuit regulating temperature-evoked posture dynamics in
054 the nematode *Caenorhabditis elegans*. Neuroscience Research. 2023;188: 10–27.
055 doi:10.1016/j.neures.2022.11.001

056 98. O'Halloran DM, Altshuler-Keylin S, Zhang X-D, He C, Morales-Phan C, Yu Y, et al. Contribution
057 of the cyclic nucleotide gated channel subunit, CNG-3, to olfactory plasticity in Caenorhabditis
058 elegans. Sci Rep. 2017;7. doi:10.1038/s41598-017-00126-7

059 99. Peng C, Rich ED, Varnum MD. Subunit Configuration of Heteromeric Cone Cyclic Nucleotide-
060 Gated Channels. Neuron. 2004;42: 401–410. doi:10.1016/S0896-6273(04)00225-9

061 100. Shuart NG, Haitin Y, Camp SS, Black KD, Zagotta WN. Molecular mechanism for 3:1 subunit
062 stoichiometry of rod cyclic nucleotide-gated ion channels. Nat Commun. 2011;2: 457.
063 doi:10.1038/ncomms1466

064 101. Zhong H, Molday LL, Molday RS, Yau K-W. The heteromeric cyclic nucleotide-gated channel
065 adopts a 3A:1B stoichiometry. Nature. 2002;420: 193–198. doi:10.1038/nature01201

066 102. Coburn CM, Bargmann CI. A Putative Cyclic Nucleotide–Gated Channel Is Required for
067 Sensory Development and Function in C. elegans. Neuron. 1996;17: 695–706.
068 doi:10.1016/S0896-6273(00)80201-9

069 103. Yuan C, Gerhards L, Solov'yov IA, Dedek K. Biotin-cGMP and -cAMP are able to permeate
070 through the gap junctions of some amacrine cells in the mouse retina despite their large size.
071 Front Ophthalmol. 2024;3. doi:10.3389/fopht.2023.1334602

072 104. Moore KB, Mitchell CK, Lin Y-P, Lee Y-H, Shihabeddin E, O'Brien J. Localized Calcium
073 Signaling and the Control of Coupling at Cx36 Gap Junctions. eNeuro. 2020;7.
074 doi:10.1523/ENEURO.0445-19.2020

075 105. Vaughn MJ, Haas JS. On the Diverse Functions of Electrical Synapses. Front Cell Neurosci.
076 2022;16. doi:10.3389/fncel.2022.910015

077 106. Jin EJ, Park S, Lyu X, Jin Y. Gap junctions: historical discoveries and new findings in the
078 Caenorhabditis elegans nervous system. Biology Open. 2020;9: bio053983.
079 doi:10.1242/bio.053983

080 107. Liu S, Schulze E, Baumeister R. Temperature- and Touch-Sensitive Neurons Couple CNG and
081 TRPV Channel Activities to Control Heat Avoidance in Caenorhabditis elegans. PLOS ONE.
082 2012;7: e32360. doi:10.1371/journal.pone.0032360

083 108. Brenner S. The genetics of Caenorhabditis elegans. Genetics. 1974;77: 71–94.
084 doi:10.1093/genetics/77.1.71

085 109. Rabinowitch I, Upadhyaya B, Pant A, Galski D, Kreines L, Bai J. Circumventing neural damage
086 in a *C. elegans* chemosensory circuit using genetically engineered synapses. Cell Systems.
087 2021;12: 263-271.e4. doi:10.1016/j.cels.2020.12.003

088 110. Frøkjær-Jensen C, Davis MW, Ailion M, Jorgensen EM. Improved Mos1-mediated transgenesis
089 in C. elegans. Nat Methods. 2012;9: 117–118. doi:10.1038/nmeth.1865

090 111. Zhang L, Wang Y, Dong Y, Pant A, Liu Y, Masserman L, et al. The endophilin curvature-sensitive
091 motif requires electrostatic guidance to recycle synaptic vesicles in vivo. Developmental Cell.
092 2022;57: 750-766.e5. doi:10.1016/j.devcel.2022.02.021

093 112. Ghanta KS, Ishidate T, Mello CC. Microinjection for precision genome editing in *Caenorhabditis*
094 *elegans*. STAR Protocols. 2021;2: 100748. doi:10.1016/j.xpro.2021.100748

095 113. Paix A, Folkmann A, Rasoloson D, Seydoux G. High Efficiency, Homology-Directed Genome
096 Editing in Caenorhabditis elegans Using CRISPR-Cas9 Ribonucleoprotein Complexes.
097 Genetics. 2015;201: 47–54. doi:10.1534/genetics.115.179382

098 114. He S, Cuentas-Condori A, Miller DM. NATF (Native and Tissue-Specific Fluorescence): A
099 Strategy for Bright, Tissue-Specific GFP Labeling of Native Proteins in Caenorhabditis elegans.
100 Genetics. 2019;212: 387–395. doi:10.1534/genetics.119.302063

101